Congruent demographic responses to Pleistocene geological processes in Sumatran parachuting frogs: a comparison of target-capture and ddRADseq for population genomic analyses

Kyle A. O'Connell*[1,2], Jamie R. Oaks[3], Amir Hamidy[4], Nia Kurniawan[5], Eric N. Smith[2], Matthew K. Fujita[2]

[1]*Division of Amphibians and Reptiles, Department of Vertebrate Zoology and Global Genome Initiative, National Museum of Natural History, Smithsonian Institute, Washington, District of Columbia, 20560, USA.*
[2]*Department of Biology and Amphibian and Reptile Diversity Research Center, The University of Texas at Arlington, Arlington, Texas 76019, USA*
[3]*Department of Biological Sciences and Museum of Natural History, Auburn University, Auburn, Alabama 36849*
[4]*Zoology Division, Museum Zoologicum Bogoriense, Research Center for Biology, Indonesian Institute of Sciences. Gd. Widyasatwaloka Jl. Raya Jakarta Bogor km 46 Cibinong, Bogor, West Java, Indonesia.*
[5]*Department of Biology, Universitas Brawijaya, Jl. Veteran, Malang 65145, East Java, Indonesia.*
**Corresponding author Kyle A. O'Connell, oconnellk@si.edu*
https://orcid.org/0000-0002-0464-9259

Catastrophic events, such as volcanic eruptions, can have profound impacts on the demographic histories of resident taxa. Due to its presumed effect on biodiversity, the Pleistocene eruption of super-volcano Toba has received abundant attention. We test the effects of the Toba eruption on the diversification, genetic diversity, and demography of three co-distributed species of parachuting frogs (Genus *Rhacophorus*) on Sumatra. We generate target-capture data (~950 loci and ~440,000 bp) for three species of parachuting frogs and use these data paired with previously generated double digest restriction-site associated DNA (ddRADseq) data to estimate population structure and genetic diversity, to test for population size changes using demographic modeling, and to estimate the temporal clustering of size change events using a full-likelihood Bayesian method. We find that populations around Toba exhibit reduced genetic diversity compared with southern populations, and that these northern populations exhibit a signal of contraction around the time of the eruption (~80 kya). However, we infer a stronger signal of expansion in southern populations around ~400 kya, and at least two of the northern populations may have also expanded at this time. Taken together, this suggests that the Toba eruption precipitated population declines in northern populations, but that the demographic history of these three species was more greatly impacted by mid-Pleistocene forest expansion, supporting local rather than regional effects of the Toba eruption.

Keywords: Anuran, demographic history, glacial cycles, Sunda Shelf, Toba eruption

INTRODUCTION

Catastrophic events can shape patterns of species diversification, population genetic structure, and local demography (Schoener & Spiller, 2006; Botting, 2016). Volcanic eruptions in particular can have profound effects on species' evolutionary histories, and these events often leave signals on the genomic patterns of resident species (Gübitz et al., 2005; Crisafulli et al., 2015). One Quaternary volcanic eruption has received exceptional attention and controversy due to its presumed impact on biodiversity: the Toba 'super-eruption' (Chester et al., 1991; Rampino & Self, 1992; Yost et al., 2018). The Toba eruption occurred ~74 kya and was the world's largest Quaternary explosive eruption (Ninkovich et al., 1978; Oppenheimer, 2002; Williams, 2011). Although the Toba Caldera experienced four major eruptions beginning at 1.2 Ma (Chesner et al., 1991), the final eruption was 3,500 times greater than the largest recent eruption (1815 eruption of Tambora) and ash deposits have been identified as far away as India and the South China Sea (Rose & Chesner, 1987; Acharyya & Basu, 1993; Westgate et al., 1998; Bühring & Sarnthein, 2000; Oppenheimer, 2002; Robock et al., 2009). Nonetheless, the eruption's impact on biological life has been extensively debated, with some sources hypothesizing the onset of a global winter that decreased Earth's temperature by as much as 3–5ºC (Rampino and Self 1992), leading to severe desiccation and pronounced deforestation (Robock et al., 2009; Williams et al., 2009; but see Haslam & Petraglia, 2010). This climate event may have driven local bottlenecks and even extinction (Robock et al., 2009), and has been implicated in precipitating human diversification (Ambrose 1998; 2003; Rampino & Self 1992).

Alternatively, studies of non-human animals, as well as some human studies, support mixed effects of the eruption on evolutionary processes (Gathorne-Hardy & Harcourt-Smith, 2003; Yost et al., 2018). The eruption has been implicated in a wide variety of evolutionary scenarios, including decreased gene flow in orangutans (Nater et al., 2011; 2017), diversification through habitat fragmentation in tigers (Luo et al., 2004), facilitating secondary contact in Sumatran elephants (Fleischer et al., 2001), and causing the extinction of one haplotype group in

palm civets (Patou et al., 2010). Alternatively, Louys (2007) and Louys and Meijaard (2010) used the fossil record to show that the eruption drove few if any species of mammals to extinction. Thus, the Toba eruption may have significantly affected human populations, but had various effects on the diversification and demography of other animals (Erwin and Vogel, 1992).

In addition to active volcanism, the island of Sumatra experienced a complex geological history during the Quaternary driven by sea level fluctuations that led to both periodic connectivity to the rest of Sundaland (Java, Borneo, Malay Peninsula) and forest expansion and contraction (Cannon et al., 2009; Hall, 2009; 2012a; 2012b; Lohman et al., 2011; Iwanaga et al., 2012; Morley, 2012; Raes et al., 2014). Recent work has shown that Sundaland was likely land positive during the Pleistocene until 400 kya, but experienced cyclical sea level fluctuations approximately every 100 kya thereafter (Sarr et al., 2019). Although these glacial cycles likely minimally impacted the inter-island dispersal of montane animals (Gorog et al., 2004; Nater et al., 2011; de Bruyn et al., 2014; O'Connell et al., 2018b), montane forest expansion (Fig. 1) and contraction during glacial cycles may have promoted population expansion and gene flow within islands in forest-restricted species, which should be detectable in the demographic history of resident species (Prates et al., 2016).

While the effects of the Toba eruption and glacial cycles have been relatively well studied in mammals, few studies have investigated how these effects impacted the demographic processes of small dispersal-limited animals. One taxonomic group that can be used to address these questions are the parachuting frogs (genus *Rhacophorus*) because they are species-rich and widely distributed across Sumatra. Fifteen species of *Rhacophorus* have been described from Sumatra, and a high proportion are endemic species that diversified *in situ* on the island (Harvey et al., 2002, Streicher et al., 2012, 2014, Hamidy & Kurniati, 2015, O'Connell et al., 2018a,b). In particular three species, *R. catamitus*, *R. modestus*, and *R. poecilonotus*, are co-distributed across the island in montane stream habitats, allowing for the comparison of populations with similar life histories located proximate to and distant from the Toba eruption. Past work with these species found evidence of congruent population structure and synchronous divergence (~5 Ma) across Sumatra, suggesting similar responses to shared historical processes (O'Connell et al., 2018a). However, the same study showed that *R. catamitus* and *R. modestus* originated in northern Sumatra, while *R. poecilonotus* originated in southern Sumatra, suggesting differential responses to some geological events between *R. poecilonotus* and the other two species. Thus, although divergence was driven by Miocene geological processes in these three species, the effects of Pleistocene processes on demographic processes have not yet been investigated.

In this study we use target-capture and double digest restriction-site associated DNA (ddRADseq) data to investigate the demographic and evolutionary effects of the Toba eruption and Pleistocene forest cycles on three *Rhacophorus* species from Sumatra. We test the following hypotheses: (1) If the Toba eruption impacted the demographic history of parachuting frogs, we expect that (a) northern populations will exhibit reduced genetic diversity compared with southern populations due to local bottlenecks, and (b) genomic data will support population contraction in the northern populations ~74 kya, but expansion in the southern populations as they potentially recolonized the eruption zone after ~74 kya. (2) If cycles of forest expansion and contraction impacted the demographic history of parachuting frogs, we expect that (c) genetic diversity will be equal between populations, and (d) analyses will infer that size change events were not temporally congruent with the eruption.

MATERIALS AND METHODS

Transcriptomic data generation and analysis

Two species of *Rhacophorus* were chosen for transcriptome sequencing: *R. modestus* (MVZ 272194, JAM 9715) from Sumatra, and *R. monticola* (JAM 14420) from Sulawesi. These species were chosen to target at least one species from each of the two primary clades within *Rhacophorus* (O'Connell et al., 2018b). Whole RNA was extracted from liver samples flash frozen in RNA-later. RNA was quantified using the Agilent 2100 Bioanalyzer (Aligent Technologies, Santa Clara, CA, USA) with an RNA chip kit. Extracted RNA for each sample was sent to the Brigham Young University DNA Sequencing Center (dnasc.byu.edu) for library preparation and sequencing on a single lane of the Illumina® HiSeq 2500.

Raw reads were cleaned and *de novo* assembled into contigs using TRINITY v.2.1.1 (Grabherr et al., 2011) under default settings. We identified orthologous exons between the two species following Yang and Smith (2014). Briefly, putative coding regions were identified with TransDecoder v.2.10 (Haas et al., 2013) using the *Nanorana parkeri* genome. Redundant reads were removed with cd-hit-est v.4.64 (Li & Godzik, 2006). Bastn v.2.7.1 (Altschul et al., 1990) was used to remove contigs from each individual that were not present in both individuals. Markov clustering was performed using MCL v.1.30 (Enright et al., 2002), which clusters sequences based on the fraction and number of blast hits. A phylogenetic tree was inferred for each homolog, and finally, the data were filtered to 1-to-1 orthologs and aligned using MAFFT v.7.302 (Katoh et al., 2002). We identified 2828 orthologous transcripts and ued these to design target loci for capture.

Target capture probe design

Target sequences were designed using a custom pipeline (See Data Availability). We used blasn v.2.7.1 (Altschul et al., 1990) to blast sequences from MVZ 272194 against JAM 1420 to identify portions of sequence alignments without ambiguous sites or gaps. We retained only completely overlapping regions, then trimmed sequences to the first 1000 bp using fastx_trimmer v.0.0.13 (http://hannonlab.cshl.edu/fastx_toolkit/). We retained alignments with GC content between 40–70 percent, sequence divergence between 1–15 percent, and sequence length between 430–1000 bp. We used RepeatMasker v.4.09 (Smit et al., 2013) to remove any transcripts with repetitive content. Probes with high or low GC, or that are too divergent from the target species can perform poorly during hybridization (Bi et al., 2012; Bragg et al., 2016; Portik et al., 2016). Probes for the target sequences were synthesized by myBaits® (Arbor Biosciences, Ann Arbor, MI) using 120 bp probes with 2x tiling. The final probe set resulted in 19,950 baits targeting 955 transcript markers from two species (total = 1910 markers).

Genomic library preparation

Genomic DNA was extracted from liver and muscle tissue stored in Cell Lysis Buffer from 69 individuals (Table SI) using a standard salt-extraction method (Sambrook & Russell 2001) followed by an additional cleanup with Sera-Mag Speedbeads (Rohland & Reich 2012). Concentrations were checked on a QUBIT® 2.0 Fluorometer (Life Technologies, Grand Island, NY, USA), and size distributions were checked on a 1% Agarose gel using 1–5 µl of DNA. We fragmented 300–800 ng of DNA per sample using 2 µl of NEB dsDNA Fragmentase (New England Biolabs, Ipswich, MA) for 20–25 minutes at 37°C and prepared genomic libraries using the Kapa Hyper Prep Kit (Kapa Biosystems, Wilmington, MA) using half the manufacture's recommended reaction volumes. For our first three library groups (all species except *R.*

modestus, *R. poecilonotus*, and *R. achantharrhena*), we did not size select between adapter ligations and PCR amplification. We conducted two PCR reactions of 7–8 amplification cycles under the following conditions: 98˚C for 45 sec; 7–8 cycles of 98˚C for 30 sec, annealing temperature of 60˚C for 30 sec, 72˚C for 30 sec, final extension of 72˚C for 1 min, and final rest at 12˚C. We pooled individuals into three capture groups of 7–8 individuals. Because the size distribution of these three libraries was very wide, we decided to size select our remaining libraries using the Blue Pippin electrophoresis platform (Sage Science, Beverly, MA, USA) for fragments between 450–750 bp. Thus, with the remaining 8 capture groups, we pooled 5–7 individuals following adapter ligation, size selected the pool, then PCR amplified pools in 4–6 reactions of 8 cycles. We checked the distribution of each pooled library group on the Agilent 2100 Bioanalyzer.

Hybridization reactions

Starting with 1 µg of DNA from each pooled library group, we followed Portik et al., (2016) to utilize two variations of blocking oligos, including the myBaits® supplied blocking oligos, as well as IDT xGen blocking oligos (Integrated DNA Technologies). When using the xGen blockers, we added 2.5 µl of the B1, 1 µl of the B2, and 2 µl of the xGen blockers. We incubated hybridization reactions for 24 hours at 65˚C. We amplified hybridized DNA in three reactions of 14 PCR cycles, with the exception of the three groups that were not size selected (Table S1) which we amplified for 30–36 cycles in three reactions because initial concentrations at 14 cycles were too low. We confirmed the distribution of each capture reaction on the Agilent 2100 Bioanalyzer, and quantified total library concentration using the QUBIT. Finally, we pooled capture libraries into two sequencing groups (Table S1) which were sequenced on two lanes of (150 bp PE; lane 1 was shared with another project, see Table S1) of the Illumina® X10 at Medgenome (medgenome.com).

Genomic data processing

We demultiplexed barcoded samples using FASTX barcode splitter v.0.0.13 (http://hannonlab.cshl.edu/fastx_toolkit/), and conducted remaining data processing using the Python pipeline SECAPR v.1.14 (Andermann et al., 2018), which is an extension of the Phyluce pipeline (Faircloth, 2015). Our SECAPR pipeline followed the following steps: (1) We cleaned raw reads using TRIMMOMATIC v.0.36 (Bolger et al., 2014), hard trimming the first 10 bp and last 13 bp from each read to remove adapter sequence, and setting the other parameters as: simpleClipThreshold = 5, palindromeClipThreshold = 20, and seedMismatch = 5. We checked the quality of each sample using FastQC, and only proceeded after all samples passed QC tests. (2) We assembled cleaned reads into contigs using TRINITY v.2.1.1 (Grabherr et al., 2011). We updated SECAPR to v.1.15 and separated our target loci by species (*R. modestus* and *R. monticola*) but after finding little difference between the two references, we used *R. modestus* target sequence for all subsequent analyses. (3) We matched assembled contigs to the target sequences for each of the three focal species separately with min-coverage = 60, min-identity = 60, and used the keep-duplicates and keep-paralogs flags. We aligned the recovered markers for each species using MAFFT v.7.407 (Katoh et al., 2002). (4) We conducted reference based assembly using the reference_assembly script for each species by mapping our cleaned reads to the species-specific reference (reference type = alignment consensus). (5) We phased alleles (phase_alleles, min coverage 6x per allele) and again aligned using MAFFT (no trim and allow

ambiguous). We further filtered by removing sequences with more than 80% missing data at a locus and trimmed using GBLOCKS v.0.91b (-b2=.1 -b3=8 -b4=10 -b5=a -t=d**;** Castresana 2000). We then removed trimmed sequences shorter than 50 bp, and sequences with more than 45% missing data. We refer to this data set as 'full-locus'. All scripts used in filtering are available online (see Data Availability).

In order to optimize our alignments at the phylogenetic level (across the genus) and also to evaluate the utility of exonic sequence for population genomic analyses, we generated a second data set that we refer to as the 'exonic' data set. Rather than assembling reads then matching the assembled contigs to a reference sequence, we mapped our cleaned reads directly to our target sequences, then phased, aligned, and filtered these alignments as described above.

We called SNPs for both data sets using the *R* script fasta2vcf.R (https://github.com/gehara). To call SNPs for the exonic data set we first separated our alignments by species so that SNPs were only retained within each species; the full-locus data set was already separated by species. We report the total number of SNPs retained, the number of loci with SNPs, and the percent missing data in Table 1. Missing data was calculated following de Medeiros & Farrell (2018).

To compare population genomic parameters estimated using our two target-capture data sets to those estimated from ddRADseq data, we utilized ddRADseq-derived SNP data for all three species from O'Connell et al., (2018a). These data sets were filtered such that 70% of individuals contained a locus for it to be retained. Data set characteristics were as follows: *R. catamitus* n = 20 with 4594 SNPs and 20.7% missing data; *R. modestus* n = 10 with 1008 SNPs and 26.31% missing data, and *R. poecilonotus* n = 17 with 798 SNPs and 25.5% missing data.

Testing probe efficacy to recover population structure and estimate genetic diversity

To verify that our capture data recovered the same population structure as mitochondrial and ddRAD data from O'Connell et al., (2018a), we estimated a ML phylogeny for each of the three species for each data set using RAxML v.8.2.11 with 100 rapid bootstrap iterations, partitioning by locus and applying a single GTRCAT model to each partition. We also sought to test how well our recovered loci could reconstruct the *Rhacophorus* phylogeny using taxa from across the genus and thus concatenated all loci for the exonic data set from all species and ran RAxML as above (Supporting Information).

We estimated population genetic summary statistics for each species for the three data sets using the populations module from STACKS v.2.4 (Catchen et al., 2013), and compared the results using all SNPs and only one random SNP per locus for the two target capture data sets (Table S3).

Testing size change models

To investigate if size changes occurred in Sumatran *Rhacophorus* (indicative of catastrophic geological events), we used the diffusion approximation method implemented in δaδi (Gutenkunst, Hernandez, Williamson, & Bustamante, 2009) to analyse two-dimensional Site Frequency Spectra (2D-SFS). The folded 2D-SFS was generated from VCF files (https://github.com/isaacovercast/easySFS), and to account for missing data we projected down to smaller sample sizes for each data set (Table 3). For each data set we compared divergence with no size change and divergence with size change (to estimate expansion or contraction) using the workflow outlined by Portik et al., (2017; https://github.com/dportik/dadi_pipeline). Following Barratt et al., (2018), we ran five iterations of each model with four sets of

increasingly focused optimizations before performing final model selection. We identified the best-supported model using AIC and log likelihoods. For the target capture data sets we compared models using all SNPs and a single random SNP for each locus, but because using linked sites violates the assumptions of AIC model selection (and because results were congruent between data sets), we only report the results of a single SNP per locus in Table 3.

Estimating the timing of demographic events

We used ecoevolity v.0.3.2 (Bryant et al. 2012; Oaks, 2019) to estimate the timing and synchronicity of demographic events. Ecoevolity is a general, full-likelihood Bayesian method that can estimate temporal clustering of demographic events for several populations. To generate input files for each data set, we included the full alignments for each locus as Oaks et al., (2019a) showed that using all sites substantially improves estimates of demographic event times. We separated each alignment into northern and southern populations for each species based on the ML phylogeny (Fig. 2) for a total of six populations being compared by ecoevolity. We tested up to 13 parameter combinations (described in the Supporting Information) and implemented the following parameters in the final analysis: we applied a Dirichlet process with a concentration parameter fixed at 2.62 (mean prior probability on 3.5 demographic events across the six populations) as the prior over all the ways the timing of the population-size change of the six populations can be assigned to 1–6 events, and an exponential distribution for the prior on event times (i.e., unique times of population-size change), with a rate of 1000 (~500 Kya assuming a mutation rate of 1.42×10^{-9} substitutions per site per year). For the prior on the current effective population size (scale by the mutation rate), we used a gamma-distributed prior (shape = 3.5, scale = 0.001). For the prior on the relative effective size of the population before the size change occurred, we used our δaδi results to apply population-specific exponential distributions. On the northern populations of *R. catamitus* and *R. modestus* we applied an exponential distribution with a mean = 2, and on the southern populations applied an exponential distribution with a mean = 0.5. In *R. poecilonotus* we applied the inverse, and in all cases allowed the parameter to be estimated. We set the mutation rate equal to one and converted posterior estimates by dividing by the mutation rate of 1.42×10^{-9} substitutions per site per year, estimated for the frog genus *Leptopelis* (Allio et al., 2017). We ran 20 MCMC chains for each prior combination for each data set for 75,000 generations with a sample taken ever 50 generations. We checked for convergence and calculated median values for parameters of interest in Tracer v.1.7.1 (Rambaut et al., 2018) with a 10% burnin. Figures were produced using the accompanying Python package 'pycoevolity' v.0.2.4 with a burnin of 101 samples for each log file.

To better understand the variability in posterior estimates between data sets, we used 'simcoevolity' v.0.2.4 (Oaks et al., 2019b) within the pycoevolity package to simulate 500 data sets using the '-c' option, which simulates alignments that matched our empirical data for numbers of individuals, locus number, locus length, and patterns of missing data within each locus. This strategy allowed us to identify if differences between estimates from the datasets were due to differences in the number of sites or loci sampled, patterns of missing data within each locus. We analyzed each simulated data set using 10 chains of ecoevolity under the parameters described above for the empirical analyses, with two modifications that allowed us to test the accuracy of the program to estimate size change around the time of the Toba eruption. We applied a Dirichlet process with a concentration parameter fixed at 20 (mean prior probability on 5.3 demographic events across the six populations) as the prior over all the ways the timing of the population-size change of the six populations can be assigned to 1–6 events,

and an exponential distribution for the prior on event times with a rate of 6000 (~95 Kya when converted by mutation rate). We repeated this procedure for each of the two target-capture data sets (500 exonic and 500 full-locus with 10 chains each), and plotted the outputs using 'pyco-sumsims' of the pycoevolity package with a burnin of 500 samples per chain.

RESULTS

Target capture efficiency

We compared two assembly strategies for generating final alignments for the three focal species (Table 1). Our full-locus data sets contained varying numbers of total bp per species, ranging from 241,721 bp in *R. modestus*, to 250,616 bp in *R. catamitus* to 326,419 bp in *R. poecilonotus*. We recovered 691 loci in *R. modestus*, 711 loci in *R. poecilonotus*, and 740 loci in *R. catamitus*. Mean locus length ranged from 339 bp in *R. catamitus*, to 350 bp in *R. modestus*, and to 459 bp in *R. poecilonotus*. Missing data varied from 15% in *R. modestus* to 26% in *R. catamitus*, and to 27% in *R. poecilonotus*. Mean SNPs per locus ranged from 4.2 in *R. poecilonotus*, to 4.3 in *R. modestus*, to 4.9 in *R. catamitus*. Loci that contained at least one SNP ranged from 530 in *R. modestus*, to 532 in *R. poecilonotus*, to 600 in *R. catamitus*.

Our exonic data sets contained 440,024 total bp and 944 total loci captured in *R. catamitus* and *R. modestus* (943 loci in *R. poecilonotus*). Mean locus length equaled 466 bp in all species, and missing data ranged from 12.7% in *R. modestus*, to 14.3% in *R.* catamitus, to 15.3% in *R. poecilonotus*. Mean SNPs per locus ranged from 3.2 in *R. poecilonotus*, to 3.8 in *R. catamitus*, to 3.7 in *R. modestus*. Loci that contained at least one SNP equaled 466 loci in *R. poecilonotus*, 488 loci in *R. catamitus*, and 494 loci in *R. modestus*.

Generally, the full-locus data set generated more total SNPs, more SNPs per locus and more loci with SNPs. However, the full-locus data set had fewer total loci recovered, shorter loci, fewer individuals per alignment, and greater levels of missing data when compared with the exonic data sets (Table 1). This assembly method was also more sensitive to divergence from the reference sequence, as observed when comparing capture success between *R. modestus* (the reference species) and the other two species (Table 1).

Population structure

Within the focal species, the target-capture data recovered similar population structure to the ddRADseq data, with three well-supported populations within each species: northern, central, and southern (Fig. 2; S1). In all species the oldest cladogenetic event was inferred between the northern population and the central and southern populations, which we lump in most analyses as a single lineage.

Genetic diversity estimation

Across species, we found generally consistent results supporting higher genetic diversity in southern populations compared with northern populations (Fig. 3; Table 2). Across data sets, parameter values were consistent with the target-capture data when using all SNPs compared with only one SNP (Table S3), and between the full-locus and exonic data sets (Table 2). However, parameter estimates varied widely between the target-capture and ddRAD data sets, with lower absolute values estimated from the ddRAD data (Table 2). In *R. catamitus* and *R. modestus*, genetic diversity (across measures and data sets) was higher in the southern populations compared with the northern populations, whereas in *R. poecilonotus*, the two target-

capture data sets supported higher diversity in the northern compared with the southern population, while the ddRAD data supported higher diversity in the southern population compared with northern populations. This suggests that all three data sets recover congruent patterns for *R. catamitus* and *R. modestus*, but in *R. poecilonotus* we observe either a marker effect (capture vs. ddRAD) or a sampling effect (only two central individuals and no southern individuals; Fig. 2).

Demographic modeling of size change events

We compared divergence with and without size change for each data set (Table 3). In all data sets for *R. catamitus* and *R. modestus*, divergence with size change was strongly supported (Δ AIC > 5). However, in *R. poecilonotus*, analyses of the full-locus and exonic data sets either failed to strongly differentiate between models or found weak support for divergence without size change (ΔAIC = 3.8), while in the ddRADseq data, the size change model was only weakly supported (ΔAIC = 3.8). This suggests that the number of SNPs or the population-level sampling in *R. poecilonotus* (two central individuals and no southern individuals) were not sufficient to differentiate between these two models. We otherwise inferred consistent patterns across analyses (Table 3).

Patterns of population size change were consistent in *R. catamitus* and *R. modestus*, the southern populations always expanded and the northern populations always contracted. In both species the magnitude of southern expansion was greater than that of northern contraction. In *R. poecilonotus* we inferred the opposite signal across all data sets, with northern expansion and southern contraction, and the magnitude of southern contraction was much greater than that of northern expansion. This was consistent when including all SNPs or only one SNP, as well as in the ddRADseq data (Table 3).

Temporal clustering of demographic events

We tested a wide range of priors for each data set to ensure that our data, and not the prior distributions, were driving the observed results (Table 4). We found that the posterior distribution of demographic events times varied little between runs with different priors, but that the prior on the concentration parameter affected the posterior probability and Bayes Factor support for the number of events between runs, although the best-supported number of events did not vary widely (e.g. 3 vs. 4 events; Figs.S3,4). Nonetheless, we inferred strikingly different results when applying the same priors to different data sets (full-locus vs. exonic; Fig. 4; Table 4). After summarizing results across the twenty chains for each analysis, we found that all analyses converged for the two target capture data sets, but none converged for the ddRAD data across parameter combinations; as such we do not report estimates for the ddRAD data. Due to the uncertainty around some of our posterior estimates with the target capture data, as well as the dependence of posterior estimate conversion on an accurate mutation rate for parameter conversion, we suggest that posterior estimates should be approached with caution.

In the full-locus data set, three demographic events received the highest posterior probability (PP = 0.35; Fig. 4A). The analysis inferred two general clusters of events, which were consistent with one event shared by the northern populations (~80 kya), and one event shared by the southern populations (~400 kya; Fig. 4C). This result was consistent between runs (Fig. S3). However, we inferred a bimodal distribution for the posterior estimates of the timing of the population-size change of northern *R. catamitus* and *R. modestus*, suggesting (1) low support for two demographic events, (2) that our data had little power to distinguish the timing of

events in these populations, or (3) these populations experienced two population size changes in the past, and because ecoevolity only models one, the posterior is 'split' between them. We report the median time estimate for each demographic event, except in the case of bimodal distributions we report the median time of each peak, and the highest posterior density (HPD) interval of both peaks. Size changes were inferred for northern *R. catamitus* at 88.0 kya and 410 kya (95% HPD = 6.7–9,155 kya), *R. modestus* at 89.4 kya and 410 kya (27.5–683.1 kya), and northern *R. poecilonotus* at 66.2 kya (0.025–204.2 kya). In southern populations size changes were inferred for *R. catamitus* at 408.5 kya (295.8–514.1 kya), in *R. modestus* at 422.5 kya (338.0–528.5 kya), and in *R. poecilonotus* at 422.5 kya (77.4–985.9 kya). The analysis inferred expansion in all populations except southern *R. poecilonotus*, and possibly in the southern population of the other two species. In all three species estimates of current effective population sizes encompassed far less uncertainty in the southern populations compared with the northern populations, and the magnitude of size change was much greater in southern than northern populations (Table 4).

In the exonic data set, four demographic events received the highest posterior probability (PP = 0.42; Fig. 4B). The analysis inferred three clusters of events, the most recent shared by northern *R. catamitus* (112.6 kya, 64.5–104.8 kya) and northern *R. poecilonotus* (119.7 kya; 84.5–140.8 kya), an older event in southern *R. catamitus* (253.5 kya, 190.1–395.2 kya), and the oldest group of events including northern and southern *R. modestus* (387.3 kya, 345.1–429.6 kya) and southern *R. poecilonotus* (366.2 kya, 84.5–704.2 kya; Fig. 4D). We again inferred expansion in all populations except southern *R. poecilonotus*. The magnitude of change was greater in southern populations than northern populations, except in *R. poecilonotus* (Table 4).

Simulations revealed that in both data sets ecoevolity struggled to accurately estimate the event times (Fig. S5). This was consistent with the findings of Oaks et al. (2019c), who found the estimation of the timing and sharing of population-size changes to be much more challenging than population divergences. Between the two data sets, the exonic data had a higher proportion of estimates for which the 95% credible interval contained the true value $p(t \in \text{CI})$, but the difference was minor (0.863 vs. 0.854; Fig. S5). This suggests that differences observed between estimates from the empirical datasets are not due to differences in the number of sites or loci sampled, or missing data patterns, but rather may be due to differences in signal from the sampled character patterns. These signals could be driven by biological factors such as selection, or data collection patterns such as paralogy and acquisition biases. When comparing the true number of events to the estimated number of events, in both data sets, ecoevolity tended to overestimate the number of events, but the proportion of estimates for which the 95% credible interval contained the true value was high in both data sets (>0.98; Fig. S6). Finally, our simulated data estimated ancestral population sizes close to the true values. Although more variation is present in the descendant population estimates, the estimated values approximate the true values somewhat; $p(t \in \text{CI}) = 0.884, 0.889$ for full-locus and exonic respectively, giving us more confidence in the direction of size change.

DISCUSSION

Comparing target capture data to ddRADseq data for population genomic studies

Studies comparing target-capture data to ddRADseq data for phylogenomic inference generally find that the two data types perform similarly for estimating phylogenies, although performance may differ at deeper, as well as recent nodes (Leaché et al., 2015; Collins & Hrbek,

2015; Harvey et al., 2016; Manthey et al., 2016). However, few studies have evaluated possible differences between data types for estimating demographic parameters. A number of factors may affect population genomic analyses such as parameter estimates and demographic modeling, particularly those that depend on the allele frequency spectrum (Harvey et al., 2016). In particular, levels of missing data and information content per locus (Collins & Hrbek, 2015) may affect both model selection and parameter estimation, but this has not been quantified by direct side-by-side studies. Unfortunately, because the sampling in our study is not exactly matched at the individual level, it is difficult to parse out the possible reasons for observed discrepancies between data sets. Our data does allow us to assert that parameter estimation between the two data types was congruent, but absolute values of estimates of genetic diversity were higher based on the target capture data. We hypothesize that this may be due to the higher information content of the target capture loci, but it also may be attributable to differences between the types of SNPs generated from protein-coding genes and random ddRADseq-derived SNPs.

Demographic impacts of the Toba eruption on northern Sumatran *Rhacophorus*

Our results across data sets support a measurable demographic effect on northern populations attributable to the Toba eruption (Figs. 3,4; Tables 3,4). Both δaδi and ecoevolity supported size change models for the northern populations of all three species, however, for *R. catamitus* and *R. modestus* δaδi supported weak contraction while ecoevolity supported weak expansion. This conflict could simply be explained by differences in the analyses or programs, or low power in our data to estimate size changes during specific windows of time. For example, ecoevolity may have more information about older events because more coalescent events have accumulated since the size change occurred, while having less accuracy to estimate the magnitude of change at more recent time scales. Alternatively, both our δaδi model and ecoevolity assumed a single instantaneous size change event, which is clearly unrealistic considering the complexity of the geological history of the region. Yet this assumption may have hindered our efforts to understand the timing and directionality of size change.

From a biological perspective, this conflict could be explained by the possible occurrence of two size change events in these species, one at the time of the southern population expansion ~400 kya, and the other occurring around the time of the Toba eruption ~80 kya (Fig. 2), thus resulting in the analysis detecting only a weak size change signal (the more recent event overriding the signal of the older event). In *R. poecilonotus* we inferred minor contraction using δaδi and minor expansion using ecoevolity but did not recover the bimodal distribution of the other two species in ecoevolity (Fig. 2). Although speciation in all three species occurred long before the Pleistocene, their non-congruent responses to Pleistocene events may be explained in part by their differing evolutionary histories, where *R. catamitus* and *R. modestus* originated in northern Sumatra, and *R. poecilonotus* originated in central or southern Sumatra (O'Connell et al., 2018a). Such differences in their response to geological processes may reflect yet unidentified differences in biological traits (Papadopoulou & Knowles 2016; Zamudio et al., 2016), perhaps driven by local adaptation to different parts of Sumatra in the early stages of divergence.

Our data does not allow us to directly assess the impact of the Toba eruption on local extinction, although past studies have shown that the eruption resulted in few extinctions (Louys 2007; Louys and Meijaard 2010). In addition, studies on the impacts of Holocene eruptions observed high survivorship and rapid recolonization in small-bodied animals including amphibians (Burt 1961; Carson et al., 1990; Crisafulli et al., 2015). However, our data concord

well with past studies supporting a bottleneck that reduced local genetic diversity (Ambrose 1996; Rampino & Ambrose 2000; Rampino & Self 1993a, 1993b; Nater et al., 2011; 2017). In addition, many studies such as this one have attributed demographic changes or pulses in diversification to the Toba eruption (Louys et al., 2004; Nater et al., 2011; 2017). Nonetheless, Toba was only one of many eruptions on Sumatra during the Pleistocene and Holocene that may have impacted diversification and demography of resident taxa (Oppenheimer, 2002), and this should be accounted for when studying local demography. Although implicated as the possible cause of evolutionary events using available data (Patou et al., 2010; Wilting et al., 2012), the increase of genomic sequence for Sumatran taxa will allow for more precise hypothesis testing of the effects of volcanic eruptions on the island.

Demographic impacts of forest expansion

As expected, we found across data sets that southern populations exhibited higher rates of genetic diversity than northern populations (Fig. 2). The only exception was in *R. poecilonotus* where the northern population exhibited higher rates of diversity in the target capture data sets, but we attribute this to sampling because we lacked southern individuals (only two central individuals were sampled). In the ddRAD data this pattern reversed when southern individuals are included. We expect that as more island-wide (and genome-wide) data sets are generated, disparities between the genetic diversity of northern and southern populations will be commonly identified.

Although we expected to find these differences in genetic diversity, we did not expect to recover a strong signal of size change in the three southern populations much earlier than the Toba eruption (~400 kya; Fig. 4), and no demographic signal of the Toba eruption in these southern populations (Fig. 4). This calls into question studies that posit global as compared to very local effects of the eruption, supporting the findings of Oppenheimer (2002) and others (i.e. Yost et al., 2018). We even found that this earlier size change event may have also affected northern *R. catamitus* and *R. modestus*.

We hypothesize that two processes could have driven this older size change event. First, many other eruptions occurred during the Pliocene across Sumatra and in west Java that could have driven demographic shifts in these populations (Global Volcanism Program, 2013). However, northern populations would likely not show a signal of size change at this older event if it was driven primarily by an eruption in southern Sumatra or west Java as most examples of the genetic consequences of eruptions posit localized effects (Carson et al., 1990; Brown et al., 2000; Gubitz et al., 2005; Bloor et al., 2008).

The second hypothesis we propose, and which we favor herein, is that of glacial periods promoting montane forest expansion that facilitated demographic changes. Recent work has shown that due to subsidence, Sundaland was not inundated during the Pleistocene until ~400 kya (Sarr et al., 2019), with cyclical inundation repeating approximately every 100 kya thereafter (Voris 2000; Woodruff 2010). Although most studies support warmer and wetter interglacial periods with expanded lowland forests with a possible savannah corridor in eastern Sumatra (Morley and Flenley 1987; Heaney 1991; Bird et al., 2005), cooler climates prevailed during glacial periods (2–6 ºC lower than today; Van der Kaars and Dam 1995; Morley 2012). Montane forests are hypothesized to have occurred lower down-slope during glacial periods (Newsome and Flenley 1988; Stuijts et al., 1984, 1988), and it is unlikely that during these periods montane forests saw notable reductions in precipitation (Kershaw et al., 2001). Thus, we hypothesize that the first glacial period following inundation, between ~400 and ~300 kya, initiated a size change

event in all but one of our *Rhacophorus* populations as montane forests expanded down-slope. This expansion of montane habitat may have allowed populations, previously isolated until 400 kya, to disperse between mountains (Fig. 3). This hypothesis is broadly supported by the 95% HPD of demographic size change for southern populations using both data sets (~300–500 kya). In addition, our simulations suggest that older event time estimates (unscaled posterior estimates ~0.006; Fig. S5) are more dispersed than the recent event times, adding to the difficulty of pinpointing the precise timing of these older demographic events.

Nonetheless, our hypothesis of a large glacially-driven expansion event is further supported by population size changes in the Sumatran rhinoceros likely driven by sea level fluctuations (Mays et al., 2018), and opens the possibility that some of the putative 'Toba effects' proposed in past studies (i.e. Luo et al., 2004; Fleischer et al., 2001) may have been caused by forest fluctuations driven by glacial cycles rather than the Toba eruption.

ACKNOWLEDGEMENTS

We thank the Ministry of Research and Technology of the Republic of Indonesia, for granting permits for this project, and representatives of LIPI for housing specimens and facilitating permits. We thank members of the field team for helping to collect voucher specimens. We are grateful to Dr. Jimmy McGuire (MVZ), and Drs. Stefan Hertwig and Manuel Schweizer (NMB) for tissue loans. We thank Jose Maldonado for generating RNAseq data, Dan Portik for sage advice on wet lab work, Utpal Smart for help at the bench, and everyone at Smithsonian Data Science Lab (plus Vanessa González at GGI) for bioinformatics support. Finally, we thank the members of the Bell lab at the NMNH for their valuable feedback on early drafts of this manuscript. A National Science Foundation Doctoral Dissertation Improvement Grant to MKF and KAO [DEB-1701721], a Division of Environmental Biology grant to ENS and M.B. Harvey [DEB-1146324], and a Global Genome Initiative Peter Buck Postdoctoral Fellowship to KAO funded this work.

REFERENCES

Acharyya, S. K., & Basu, P. K. (1993). Toba ash on the Indian subcontinent and its implications for correlation of Late Pleistocene alluvium. *Quaternary Research*, *40*, 10–19.

Allio, R., Donega, S., Galtier, N., & Nabholz, B. (2017). Large variation in the ratio of mitochondrial to nuclear mutation rate across animals: implications for genetic diversity and the use of mitochondrial DNA as a molecular marker. *Molecular Biology and Evolution*, *34*, 2762–2772.

Altschul, S.F., Gish, W., Miller, W., Myers, E. W. & Lipman, D. J. (1990) Basic local alignment search tool. *Journal of Molecular Biology*, *215*, 403–410.

Ambrose, S. H. (1998). Late Pleistocene human population bottlenecks, volcanic winter, and differentiation of modern humans. *Journal of Human Evolution*, *34*, 623–651.

Ambrose, S. H. (2003). Did the super–eruption of Toba cause a human population bottleneck? Reply to Gathorne–Hardy and Harcourt–Smith. *Journal of Human Evolution*, *45*, 231–237.

Andermann, T., Cano, A., Zizka, A., Bacon, C., & Antonelli, A. (2018). SECAPR–A bioinformatics pipeline for the rapid and user–friendly processing of Illumina sequences, from raw reads to alignments. *PeerJ*, *6*, e5175.

Barratt, C. D., Bwong, B. A., Jehle, R., Liedtke, H. C., Nagel, P., Onstein, R. E., ... & Loader, S. P. (2018). Vanishing refuge? Testing the forest refuge hypothesis in coastal East Africa

using genome-wide sequence data for seven amphibians. *Molecular Ecology*, *27*, 4289–4308.

Bi, K., Vanderpool, D., Singhal, S., Linderoth, T., Moritz, C., & Good, J. M. (2012). Transcriptome–based exon capture enables highly cost–effective comparative genomic data collection at moderate evolutionary scales. *BMC Genomics*, *13*, 403.

Bird, M. I., Taylor, D., & Hunt, C. (2005). Palaeoenvironments of insular Southeast Asia during the Last Glacial Period: a savanna corridor in Sundaland?. *Quaternary Science Reviews*, *24*, 2228–2242.

Bloor, P., Kemp, S. J., & Brown, R. P. (2008). Recent volcanism and mitochondrial DNA structuring in the lizard Gallotia atlantica from the island of Lanzarote. *Molecular Ecology*, *17*, 854–866.

Bolger, A. M., Lohse, M., & Usadel, B. (2014). Trimmomatic: a flexible trimmer for Illumina sequence data. *Bioinformatics*, *30*, 2114–2120.

Botting, J. P. (2002). The role of pyroclastic volcanism in Ordovician diversification. *Geological Society, London, Special Publications*, *194*, 99–113.

Bragg, J. G., Potter, S., Bi, K., & Moritz, C. (2016). Exon capture phylogenomics: efficacy across scales of divergence. *Molecular Ecology Resources*, *16*, 1059–1068.

Bryant, D., Bouckaert, R., Felsenstein, J., Rosenberg, N. A., & RoyChoudhury, A. (2012). Inferring species trees directly from biallelic genetic markers: bypassing gene trees in a full coalescent analysis. *Molecular Biology and Evolution*, *29*, 1917–1932.

Brown, R. P., Campos–Delgado, R., & Pestano, J. (2000). Mitochondrial DNA evolution and population history of the Tenerife skink Chalcides viridanus. *Molecular Ecology*, *9*, 1061–1067.

Bühring, C., & Sarnthein, M. (2000). Toba ash layers in the South China Sea: evidence of contrasting wind directions during eruption ca. 74 ka. *Geology*, *28*, 275–278.

Burt, W. H. (1961). Some effects of Volcan Parcutin on vertebrates. *Occasional Papers of the Museum of Zoology University of Michigan*, *620*, 1–24.

Cannon, C. H., Morley, R. J., & Bush, A. B. (2009). The current refugial rainforests of Sundaland are unrepresentative of their biogeographic past and highly vulnerable to disturbance. *Proceedings of the National Academy of Sciences*, *106*, 11188–11193.

Carson, H. L., Lockwood, J. P., & Craddock, E. M. (1990). Extinction and recolonization of local populations on a growing shield volcano. *Proceedings of the National Academy of Sciences*, *87*, 7055–7057.

Castresana, J. (2000). Selection of conserved blocks from multiple alignments for their use in phylogenetic analysis. *Molecular Biology and* Evolution, *17*, 540–552.

Catchen, J., Hohenlohe, P. A., Bassham, S., Amores, A., & Cresko, W. A. (2013). Stacks: an analysis tool set for population genomics. *Molecular Ecology*, *22*, 3124–3140.

Chesner, C., Rose, W. I., Deino, A. L., Drake, R., & Westgate, J. A. (1991). Eruptive history of Earth's largest Quaternary caldera (Toba, Indonesia) clarified. *Geology*, *19*, 200–203.

Collins, R. A., & Hrbek, T. (2015). An in silico comparison of reduced–representation and sequence–capture protocols for phylogenomics. *BioRxiv*.doi: 10.1101/032565

Crisafulli, C. M., Swanson, F. J., Halvorson, J. J., & Clarkson, B. D. (2015). Volcano ecology: Disturbance characteristics and assembly of biological communities. In *The Encyclopedia of Volcanoes* (pp. 1265–1284). Academic Press.

de Bruyn, M., Stelbrink, B., Morley, R. J., Hall, R., Carvalho, G. R., Cannon, C. H., ... & Maiorano, L. (2014). Borneo and Indochina are major evolutionary hotspots for Southeast Asian biodiversity. *Systematic Biology*, *63*, 879–901.

de Medeiros, B. A., & Farrell, B. D. (2018). Whole-genome amplification in double-digest RADseq results in adequate libraries but fewer sequenced loci. *PeerJ*, *6*, e5089.

Enright, A. J., Van Dongen, S., & Ouzounis, C. A. (2002). An efficient algorithm for large–scale detection of protein families. *Nucleic Acids Research*, *30*, 1575–1584.

Erwin, D. H., & Vogel, T. A. (1992). Testing for causal relationships between large pyroclastic volcanic eruptions and mass extinctions. *Geophysical Research Letters*, *19*, 893–896.

Faircloth, B. C. (2015). PHYLUCE is a software package for the analysis of conserved genomic loci. *Bioinformatics*, *32*, 786–788.

Fleischer, R. C., Perry, E. A., Muralidharan, K., Stevens, E. E., & Wemmer, C. M. (2001). Phylogeography of the Asian elephant (*Elephas maximus*) based on mitochondrial DNA. *Evolution*, *55*, 1882–1892.

Gathorne–Hardy, F. J., & Harcourt–Smith, W. E. H. (2003). The super–eruption of Toba, did it cause a human bottleneck?. *Journal of Human Evolution*, *45*, 227–23.

Gorog, A. J., Sinaga, M. H., & Engstrom, M. D. (2004). Vicariance or dispersal? Historical biogeography of three Sunda shelf murine rodents (*Maxomys surifer*, *Leopoldamys sabanus* and *Maxomys whiteheadi*). *Biological Journal of the Linnean Society*, *81*, 91–109.

Global Volcanism Program, 2013. Volcanoes of the World, v.4.8.2. Venzke, E (ed.). Smithsonian Institution. Downloaded 28 Aug 2019. https://doi.org/10.5479/si.GVP.VOTW4–2013.

Grabherr, M. G., Haas, B. J., Yassour, M., Levin, J. Z., Thompson, D. A., Amit, I., ... & Chen, Z. (2011). Trinity: reconstructing a full–length transcriptome without a genome from RNA–Seq data. *Nature Biotechnology*, *29*, 644–652.

Gübitz, T., Thorpe, R. S., & Malhotra, A. (2005). The dynamics of genetic and morphological variation on volcanic islands. *Proceedings of the Royal Society B: Biological Sciences*, *272*, 751–757.

Gutenkunst, R. N., Hernandez, R. D., Williamson, S. H., & Bustamante, C. D. (2009). Inferring the joint demographic history of multiple populations from multidimensional SNP frequency data. *PLoS Genetics*, *5*, e1000695.

Haas, B. J., Papanicolaou, A., Yassour, M., Grabherr, M., Blood, P. D., Bowden, J., ... & MacManes, M. D. (2013). De novo transcript sequence reconstruction from RNA–seq using the Trinity platform for reference generation and analysis. *Nature Protocols*, *8*, 1494–1512.

Hall, R. (2009). Southeast Asia's changing palaeogeography. *Blumea – Biodiversity, Evolution and Biogeography of Plants*, *54*, 148–161.

Hall, R. (2012a). Late Jurassic–Cenozoic reconstructions of the Indonesian region and the Indian Ocean. *Tectonophysics*, *570*, 1–41.

Hall, R. (2012b). A review of the Cenozoic palaeoclimate history of Southeast Asia. In D.J. Gower, K.G. Johnson, J.E. Richardson, B.R. Rosen, L. Ruber, and S.T. Williams (Eds.), *Biotic Evolution and Environmental Change in Southeast Asia*. Cambridge, UK: Cambridge University Press.

Hamidy, A., & Kurniati, H. (2015). A new species of tree frog genus *Rhacophorus* from Sumatra, Indonesia Amphibia, Anura. *Zootaxa, 3947*, 49–66.

Harvey, M. B., Pemberton, A. J., Smith, E. N. (2002). New and poorly known parachuting frogs Rhacophoridae: *Rhacophorus* from Sumatra and Java. *Herpetological Monographics*, *161*, 46–92.

Harvey, M. G., Smith, B. T., Glenn, T. C., Faircloth, B. C., & Brumfield, R. T. (2016). Sequence capture versus restriction site associated DNA sequencing for shallow systematics. *Systematic Biology*, *65*, 910–924.

Haslam, M., & Petraglia, M. (2010). Comment on "Environmental impact of the 73 ka Toba super–eruption in South Asia" by MAJ Williams, SH Ambrose, S. van der Kaars, C. Ruehlemann, U. Chattopadhyaya, J. Pal and PR Chauhan [Palaeogeography, Palaeoclimatology, Palaeoecology 284 (2009) 295–314]. *Palaeogeography, Palaeoclimatology, Palaeoecology*, *296*, 199–203.

Heaney, L. R. (1991). A synopsis of climatic and vegetational change in Southeast Asia. In *Tropical Forests and Climate* (pp. 53–61). Springer, Dordrecht.

Iwanaga, H., Teshima, K. M., Khatab, I. A., Inomata, N., Finkeldey, R., Siregar, I. Z., ... & Szmidt, A. E. (2012). Population structure and demographic history of a tropical lowland rainforest tree species *Shorea parvifolia* (Dipterocarpaceae) from Southeastern Asia. *Ecology and Evolution*, *2*, 1663–1675.

Katoh, K., Misawa, K., Kuma, K. I., & Miyata, T. (2002). MAFFT: a novel method for rapid multiple sequence alignment based on fast Fourier transform. *Nucleic Acids Research*, *30*, 3059–3066.

Kershaw, A. P., Penny, D., van der Kaars, S., Anshari, G., & Thamotherampillai, A. (2001). Vegetation and climate in lowland southeast Asia at the Last Glacial Maximum. *Faunal and Floral Migrations and Evolution in SE Asia–Australasia. Balkema, Lisse*, 227–236.

Leaché, A. D., Chavez, A. S., Jones, L. N., Grummer, J. A., Gottscho, A. D., & Linkem, C. W. (2015). Phylogenomics of phrynosomatid lizards: conflicting signals from sequence capture versus restriction site associated DNA sequencing. *Genome Biology and Evolution*, *7*, 706–719.

Li, W., & Godzik, A. (2006). Cd–hit: a fast program for clustering and comparing large sets of protein or nucleotide sequences. *Bioinformatics*, *22*, 1658–1659.

Louys, J. (2007). Limited effect of the Quaternary's largest super–eruption (Toba) on land mammals from Southeast Asia. *Quaternary Science Reviews*, *26*, 3108–3117.

Louys, J. (2012). Mammal community structure of Sundanese fossil assemblages from the Late Pleistocene, and a discussion on the ecological effects of the Toba eruption. *Quaternary International*, *258*, 80–87.

Louys, J., & Meijaard, E. (2010). Palaeoecology of Southeast Asian megafauna-bearing sites from the Pleistocene and a review of environmental changes in the region. *Journal of Biogeography*, *37*, 1432–1449.

Luo, S. J., Kim, J. H., Johnson, W. E., van der Walt, J., Martenson, J., Yuhki, N., ... & Tilson, R. (2004). Phylogeography and genetic ancestry of tigers (*Panthera tigris*). *PLoS Biology*, *2*, e442.

Manthey, J. D., Campillo, L. C., Burns, K. J., & Moyle, R. G. (2016). Comparison of target–capture and restriction–site associated DNA sequencing for phylogenomics: a test in cardinalid tanagers (Aves, Genus: *Piranga*). *Systematic Biology*, *65*, 640–650.

Mays Jr, H. L., Hung, C. M., Shaner, P. J., Denvir, J., Justice, M., Yang, S. F., ... & Primerano, D. A. (2018). Genomic analysis of demographic history and ecological niche modeling in

the endangered Sumatran rhinoceros *Dicerorhinus sumatrensis*. *Current Biology*, *28*, 70–76.

Meijaard, E., 2004. Solving mammalian riddles: a reconstruction of the Tertiary and Quaternary distribution of mammals and their palaeoenvironments in island South–East Asia. *(*Australian National University, Canberra*)* PhD thesis.

Morley, R. J., & Flenley, J. R. (1987). Late Cainozoic Vegetational and Environmental Changes in the Malay Archipelago. In T. C. Whitmore (ed.), *Biogeographical Evolution in the Malay Archipelago*, Oxford Monographs in Biogeography, 4, pp. 50–59.

Morley, R. (2012). A review of the Cenozoic palaeoclimate history of Southeast Asia. In D.J. Gower, K.G. Johnson, J.E. Richardson, B.R. Rosen, L. Ruber, and S.T. Williams (Eds.), *Biotic Evolution and Environmental Change in Southeast Asia*. Cambridge, UK: Cambridge University Press.

Nater, A., Nietlisbach, P., Arora, N., van Schaik, C. P., van Noordwijk, M. A., Willems, E. P., ... & Verschoor, E. J. (2011). Sex–biased dispersal and volcanic activities shaped phylogeographic patterns of extant orangutans (genus: *Pongo*). *Molecular Biology and Evolution*, *28*, 2275–2288.

Nater, A., Mattle–Greminger, M. P., Nurcahyo, A., Nowak, M. G., De Manuel, M., Desai, T., ... & Lameira, A. R. (2017). Morphometric, behavioral, and genomic evidence for a new orangutan species. *Current Biology*, *27*, 3487–3498.

Newsome, J., & Flenley, J. R. (1988). Late Quaternary vegetational history of the Central Highlands of Sumatra. II. Palaeopalynology and vegetational history. *Journal of Biogeography*, *15*, 555–578.

Ninkovich, D., Shackleton, N. J., Abdel–Monem, A. A., Obradovich, J. D., & Izett, G. (1978). K–Ar age of the late Pleistocene eruption of Toba, north Sumatra. *Nature*, *276*, 574–577.

Oaks, J. R. (2019). Full Bayesian comparative phylogeography from genomic data. *Systematic biology*, *68*, 371–395.

Oaks, J. R., L'Bahy, N., & Cobb, K. A. (2019a). Insights from a general, full–likelihood Bayesian approach to inferring shared evolutionary events from genomic data: Inferring shared demographic events is challenging. *bioRxiv*, 679878.

Oaks, J. R., Siler, C. D., & Brown, R. M. (2019b). The comparative biogeography of Philippine geckos challenges predictions from a paradigm of climate-driven vicariant diversification across an island archipelago. *Evolution*, *73*, 1151–1167.

O'Connell, K. A., Hamidy, A., Kurniawan, N., Smith, E. N., & Fujita, M. K. (2018a). Synchronous diversification of parachuting frogs (Genus *Rhacophorus*) on Sumatra and Java. *Molecular Phylogenetics and Evolution*, *123*, 101–112.

O'Connell, K. A., Smart, U., Smith, E. N., Hamidy, A., Kurniawan, N., & Fujita, M. K. (2018b). Within-island diversification underlies parachuting frog (Rhacophorus) species accumulation on the Sunda Shelf. *Journal of Biogeography*, *45*, 929–940.

Oppenheimer, C. (2002). Limited global change due to the largest known Quaternary eruption, Toba≈ 74 kyr BP?. *Quaternary Science Reviews*, *21*, 1593–1609.

Papadopoulou, A., & Knowles, L. L. (2016). Toward a paradigm shift in comparative phylogeography driven by trait-based hypotheses. *Proceedings of the National Academy of Sciences*, *113*, 8018-8024.

Patou, M. L., Wilting, A., Gaubert, P., Esselstyn, J. A., Cruaud, C., Jennings, A. P., ... & Veron, G. (2010). Evolutionary history of the *Paradoxurus* palm civets–a new model for Asian biogeography. *Journal of Biogeography*, *37*, 2077–2097.

Pestano, J., & Brown, R. P. (1999). Geographical structuring of mitochondrial DNA in Chalcides sexlineatus within the island of Gran Canaria. *Proceedings of the Royal Society of London. Series B: Biological Sciences*, *266*, 805–812.

Portik, D. M., Smith, L. L., & Bi, K. (2016). An evaluation of transcriptome-based exon capture for frog phylogenomics across multiple scales of divergence (Class: Amphibia, Order: Anura). *Molecular Ecology Resources*, *16*, 1069–1083.

Prates, I., Xue, A. T., Brown, J. L., Alvarado–Serrano, D. F., Rodrigues, M. T., Hickerson, M. J., & Carnaval, A. C. (2016). Inferring responses to climate dynamics from historical demography in neotropical forest lizards. *Proceedings of the National Academy of Sciences*, *113*, 7978–7985.

Rambaut, A., Drummond, A. J., Xie, D., Baele, G., & Suchard, M. A. (2018). Posterior summarisation in Bayesian phylogenetics using Tracer 1.7. *Systematic Biology*, *67*, 901–904.

Rose, W. I., & Chesner, C. A. (1987). Dispersal of ash in the great Toba eruption, 75 ka. *Geology*, *15*, 913–917.

Raes, N., Cannon, C. H., Hijmans, R. J., Piessens, T., Saw, L. G., Van Welzen, P. C., & Slik, J. F. (2014). Historical distribution of Sundaland's Dipterocarp rainforests at Quaternary glacial maxima. *Proceedings of the National Academy of Sciences*, *111*, 16790–16795.

Rampino, M. R., & Self, S. (1992). Volcanic winter and accelerated glaciation following the Toba super–eruption. *Nature*, *359*, 50–52.

Rampino, M. R., & Self, S. (1993a). Bottleneck in human evolution and the Toba eruption. *Science*, *262*, 1955–1955.

Rampino, M. R., & Self, S. (1993b). Climate–volcanism feedback and the Toba eruption of ~74,000 years ago. *Quaternary Research*, *40*, 269–280.

Rampino, M. R., & Ambrose, S. H. (2000). Volcanic winter in the Garden of Eden: The Toba supereruption and the late Pleistocene human population crash, in McCoy, F. W., and Heiken, G., eds., *Volcanic Hazards and Disasters in Human Antiquity*: Boulder, Colorado, Geological Society of America Special Paper 345.

Robock, A., Ammann, C. M., Oman, L., Shindell, D., Levis, S., & Stenchikov, G. (2009). Did the Toba volcanic eruption of ~74 ka BP produce widespread glaciation?. *Journal of Geophysical Research: Atmospheres*, *114*, D10107.

Rohland, N., Reich, D. (2012). Cost–effective, high–throughput DNA sequencing libraries for multiplexed target capture. *Genome Research*, *22*, 939–946.

Sarr, A. C., Husson, L., Sepulchre, P., Pastier, A. M., Pedoja, K., Elliot, M., ... & Aribowo, S. (2019). Subsiding Sundaland. *Geology*, *47*, 119–122.

Sambrook, J., Russell, D. (2001) Molecular Cloning: A Laboratory Manual, 3rd Edition. Cold Spring Harbor, NY: Cold Spring Harbor Laboratory Press.

Schoener, T. A., Spiller, D. A. (2006). Nonsynchronous recovery of community characteristics in island spiders after a catastrophic hurricane. *Proceedings of the National Academy of Sciences*, *103*, 2220–2225.

Smit, AFA, Hubley, R & Green, P. *RepeatMasker Open-4.0*. 2013-2015 <http://www.repeatmasker.org>.

Streicher, J. W., Harvey, M. B., Sheehy, C. M. III, Anders, B., Smith, E. N. (2012). Identification and description of the tadpole of the parachuting frog *Rhacophorus catamitus* from southern Sumatra, Indonesia. *Journal of Herpetology*, *46*, 503–506.

Streicher, J. W., Hamidy, A., Harvey, M. B., Anders, B., Shaney, K. J., Kurniawan, N., Smith, E.

N. (2014). Mitochondrial DNA reveals a new species of parachuting frog (Rhacophoridae: *Rhacophorus*) from Sumatra. *Zootaxa*, *3878*, 351–356.

Stuijts, I., (1984). Palynological Study of Situ Bayongbong, West Java. *Modern Quaternary Research, South East Asia*, *8*, 17–28.

Stuijts, I., Newsome, J. C., & Flenley, J. R. (1988). Evidence for late Quaternary vegetational change in the Sumatran and Javan highlands. *Review of Palaeobotany and Palynology*, *55*, 207–216.

Tougard, C., & Montuire, S. (2006). Pleistocene paleoenvironmental reconstructions and mammalian evolution in South–East Asia: focus on fossil faunas from Thailand. *Quaternary Science Reviews*, *25*, 126–141.

Van der Kaars, W. A., & Dam, M. A. C. (1995). A 135,000–year record of vegetational and climatic change from the Bandung area, West–Java, Indonesia. *Palaeogeography, Palaeoclimatology, Palaeoecology*, *117*, 55–72.

Voris, H. K. (2000). Maps of Pleistocene sea levels in Southeast Asia: shorelines, river systems and time durations. *Journal of Biogeography*, *27*, 1153–1167.

Westgate, J. A., Shane, P. A., Pearce, N. J., Perkins, W. T., Korisettar, R., Chesner, C. A., ... & Acharyya, S. K. (1998). All Toba tephra occurrences across peninsular India belong to the 75,000 yr BP eruption. *Quaternary Research*, *50*, 107–112.

Williams, M. A., Ambrose, S. H., van der Kaars, S., Ruehlemann, C., Chattopadhyaya, U., Pal, J., & Chauhan, P. R. (2009). Environmental impact of the 73 ka Toba super–eruption in South Asia. *Palaeogeography, Palaeoclimatology, Palaeoecology*, *284*, 295–314.

Wilting, A., Sollmann, R., Meijaard, E., Helgen, K. M., & Fickel, J. (2012). Mentawai's endemic, relictual fauna: is it evidence for Pleistocene extinctions on Sumatra?. *Journal of Biogeography*, *39*, 1608–1620.

Woodruff, D. S. (2010). Biogeography and conservation in Southeast Asia: how 2.7 million years of repeated environmental fluctuations affect today's patterns and the future of the remaining refugial–phase biodiversity. *Biodiversity and Conservation*, *19*, 919–941.

Yang, Y. & Smith, S. A. (2014). Orthology inference in non–model organisms using transcriptomes and low–coverage genomes: improving accuracy and matrix occupancy for phylogenomics. *Molecular Biology and Evolution*, *31*, 3081-3092.

Yost, C. L., Jackson, L. J., Stone, J. R., & Cohen, A. S. (2018). Subdecadal phytolith and charcoal records from Lake Malawi, East Africa imply minimal effects on human evolution from the~ 74 ka Toba supereruption. *Journal of Human Evolution*, *116*, 75–94.

Zamudio, K. R., Bell, R. C., & Mason, N. A. (2016). Phenotypes in phylogeography: Species' traits, environmental variation, and vertebrate diversification. *Proceedings of the National Academy of Sciences*, *113*, 8041–8048.

DATA ACCESSIBILITY

Double-digest RADseq data from O'Connell et al., (2018a) can be found at SAMN05426771–SAMN05426803, and SAMN08437163–SAMN08437177. Demultiplexed raw data from the target capture data can be found at SRA XXX [deposited after acceptance]. Workflow for transcriptome-based capture probe design can be found at: https://github.com/kyleaoconnell22/Exome_Capture_Probe_Design.git
Workflow for filtering locus alignments post SECAPR/PHYLUCE (https://github.com/kyleaoconnell22/TargetCaptureAnalyses).

Alignment files and ecoevolity configuration files are available at Figshare doi XXX [deposited after acceptance].

AUTHOR CONTRIBUTION

E.N.S., A.H., N.K. and K.A.O. conducted fieldwork; K.A.O. and M.F.K. conducted laboratory work; K.A.O. and M.F.K. procured funding, K.A.O. analyzed the data; K.A.O. led the writing, and all authors approved of the final version of the manuscript.

TABLES

Table 1: Summary statistics of target capture data sets for each species. Abbreviations are as follows: Total bp = length of alignment, Seqs/aln = the number of individual samples included in the alignment, % missing = the percent missing data for each alignment, Loci/SNP = the number of loci with a variant site for that species.

Species	Data set	Total bp	#Loci	Seqs/aln	Mean Length (bp)	%missing	Total SNPs	Loci w/ SNP	SNPs/locus
catamitus	Full-locus	250616	740	10.75	338.7	25.5	2935	600	4.89
	Exonic	440024	944	11.25	466	14.25	1836	488	3.76
modestus	Full-locus	241721	691	7.9	349.8	15	2261	530	4.27
	Exonic	440024	944	8.1	466	12.7	2336	494	4.73
poecilonotus	Full-locus	326419	711	5.95	459	27	2237	532	4.20
	Exonic	440024	943	6.95	466.5	15.3	1533	466	3.29

Table 2: Population-level summary statistics for each species and data set. Abbreviations are as follows: MeanN/locus = average number of samples in the alignment for a given locus, Private/N = The number of private alleles divided by the average number of individuals per alignment to correct for sampling bias in private allele estimation, %Poly = the percent of sites in a locus that are polymorphic, Ho = observed heterozygosity, He = estimated heterozygosity, Obs Hom = Observed homozygosity.

Species	Assembly	Pop ID	MeanN/locus	Private alleles	Private/N	#SNPs	Variant sites	%Poly	Ho	He	Obs Hom	Pi
catamitus	Full-locus	south	7.6	342	45	596	583	63.6	0.12	0.16	0.88	0.17
		north	3	143	48	592	580	29.9	0.1	0.1	0.9	0.13
	Exonic	south	7.8	324	41.4	488	483	71.9	0.12	0.16	0.88	0.17
		north	3.2	103	31.8	482	477	25.7	0.08	0.08	0.92	0.1
	ddRAD	south	8	2915	366.6	4594	4594	66	0.07	0.16	0.93	0.17
		north	7.9	1050	132.8	4594	4594	25.4	0.06	0.07	0.94	0.08
modestus	Full-locus	south	5.8	354	61.2	530	518	70.9	0.15	0.18	0.85	0.2

		north	1.9	56	29.7	524	513	13.9	0.07	0.06	0.93	0.08
	Exonic	south	5.9	377	63.7	494	480	78.3	0.17	0.19	0.83	0.21
		north	2	48	24.1	494	480	11.7	0.06	0.05	0.94	0.06
	ddRAD	south	4	622	155.2	1008	1008	66.8	0.14	0.22	0.86	0.26
		north	3.4	163	48.5	1008	1008	21.2	0.03	0.08	0.97	0.09
poecilonotus	Full-locus	central	1.2	110	88.3	526	496	34.4	0.26	0.16	0.74	0.29
		north	4.5	286	63.2	532	501	68	0.19	0.21	0.81	0.23
	Exonic	central	1.7	136	81.1	465	444	45.6	0.23	0.19	0.77	0.29
		north	5.1	230	45.2	466	444	65.7	0.2	0.19	0.8	0.21
	ddRAD	south	5.2	415	79.4	798	798	62.9	0.1	0.19	0.9	0.21
		north	7.4	286	38.4	798	798	46.7	0.1	0.13	0.9	0.13

Table 3: Summary of demographic modeling conducted in δaδi. Alleles and sites refers to the number of alleles and sites included after downscaling. Δ AIC refers to the change in AIC value of the best size change model compared to the best model without size change. NuA = scaled population size before size change event, Nub = scaled population size after size change event.

Species	Assembly	Pop ID	Alleles	Sites	Δ AIC	NuA	Nub	Exp/Contr?
catamitus	Full-locus	south	10	306	7.64	0.42	2.57	Expansion
		north	6	111		2.75	0.39	Contraction
	Exonic	south	14	320	11.5	0.12	3.4	Expansion
		north	6	92		5.19	0.54	Contraction
	RAD	south	14	2277	109.4	0.26	2.02	Expansion
		north	14	1000		0.43	0.34	Contraction
modestus	Full-locus	south	10	344	33.5	0.5	4.83	Expansion
		north	4	71		5.68	0.2	Contraction
	Exonic	south	12	348	13.34	0.52	8.09	Expansion
		north	4	55		0.57	0.25	Contraction
	RAD	south	6	598	24.98	0.44	2.94	Expansion
		north	6	196		2.52	0.1	Contraction

poecilonotus	Full-locus	central	2	152	0	8.9	0.36	Contraction
		north	8	291		0.06	1.11	Expansion
	Exonic	central	4	173	–	21.22	0.53	Contraction
		north	10	290		0.66	12.62	Expansion
	RAD	south	8	450	3.84	8.78	0.6	Contraction
		north	14	329		0.4	1.86	Expansion

Table 4: Summary statistics from ecoevolity (Oaks 2019) analysis estimating temporal clustering of demographic events. Parameters are scaled by the mutation rate of 1.42 x 10^{-9} substitutions per site per year, estimated for the frog genus *Leptopelis* (Allio et al., 2017), and assume a one year generation time. Population sizes, including ancestral, descendent, and magnitude of expansion, are shown in the thousands of individuals. Negative expansion values represent contraction events. Scaled event times show the median values of the posterior distribution, except in the case of northern *R. catamitus* and *R. modestus* which exhibited bimodal distributions; we report the median value of the first peak for both species. The second peak, shown in Fig. 4C is synchronous with the southern populations.

Species	Assembly	Alignment length	#Events > PP	PP	Pop ID	Scaled event time (kya)	95% HDP (kya)	Scaled ancestral size	95% HDP	Scaled descendent size	95% HDP	Magnitude of expansion
catamitus	Full-locus	250616	3	0.35	south	408.5	295.8–514.1	774.6	697.2–774.6	2,535.20	2,042.3–3,309.9	1,795.80
					north	88	1.7–1,408.5	676.1	514.1–774.6	1,197.70	704.2–3,521.1	288.70
	Exonic	440024	4	0.42	south	253.5	190.1–395.2	443.7	408.5–471.8	2,535.20	1,619.7–3,736.4	2,091.50
					north	112.6	64.5–140.8	295.8	260.6–316.9	1,542.30	528.2–3,450.7	1,246.50
modestus	Full-locus	241721	3	0.35	south	422.5	338.0–528.2	535.20	493–577.5	2,746.50	2,112.7–3,662	2,284.70
					north	89.4	27.5–683.1	253.5	119.7–331	985.90	373.2–359.2	809.90

	Exonic	440024	4	0.42	south	387.3	345.1–429.6	345.1	323.9–373.2	4,577.50	3,521.1–5,985.9	4,232.40
					north	387.3	277.6–507.0	84.50	32.2–133.8	2,112.70	1,126.8–3,873.2	2,028.20
poecilonotus	Full-locus	326419	3	0.35	south	422.5	77.5–985.9	1,619.70	1,056.3–2,605.6	323.90	176.1–563.4	-1,470.90
					north	66.2	0.025–204.2	676.10	640.8–704.2	1,901.40	690.1–422.5	739.50
	Exonic	439942	4	0.42	south	366.2	84.5–704.2	1,126.80	774.6–1,971.4	323.30	105.6–366.2	-803.50
					north	119.7	84.5–140.8	366.2	345.1–380.3	4,718.30	2,464.8–7,746.5	4,352.10

FIGURES

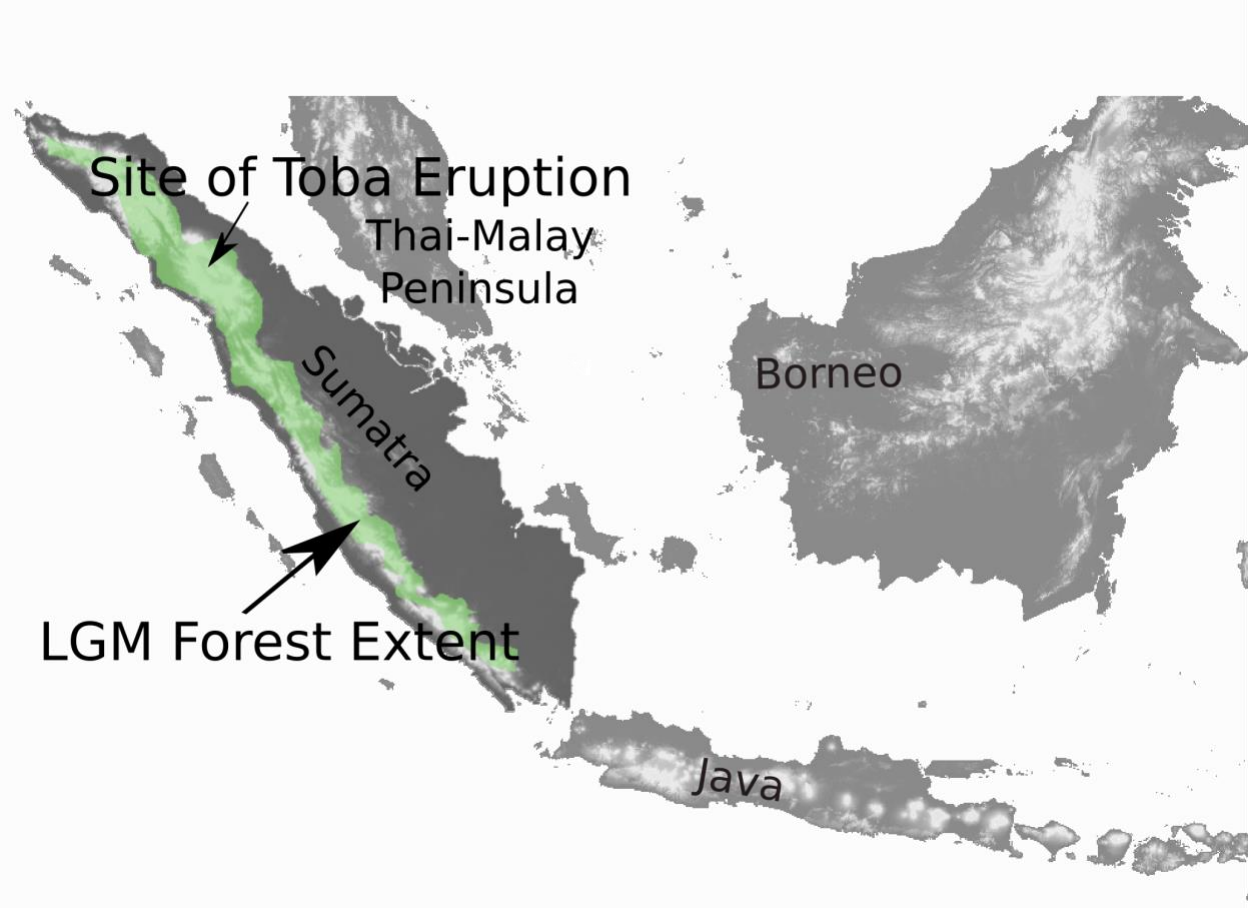

Figure 1: Map of the Sunda Shelf showing the four landmasses in the region: Sumatra, Java, Borneo and the Thai-Malay Peninsula. Within Sumatra we highlight the site of the super-volcano Toba, which erupted ~74 kya. We also highlight in green the estimated extent of montane forest habitat during the Last Glacial Maxima redrawn from the closed corridor scenario of Cannon et al., 2009. We use these estimates to roughly approximate the montane forest cover of the first glacial cycle (~350 kya) after Sumatra's first Pleistocene inundation ~400 kya.

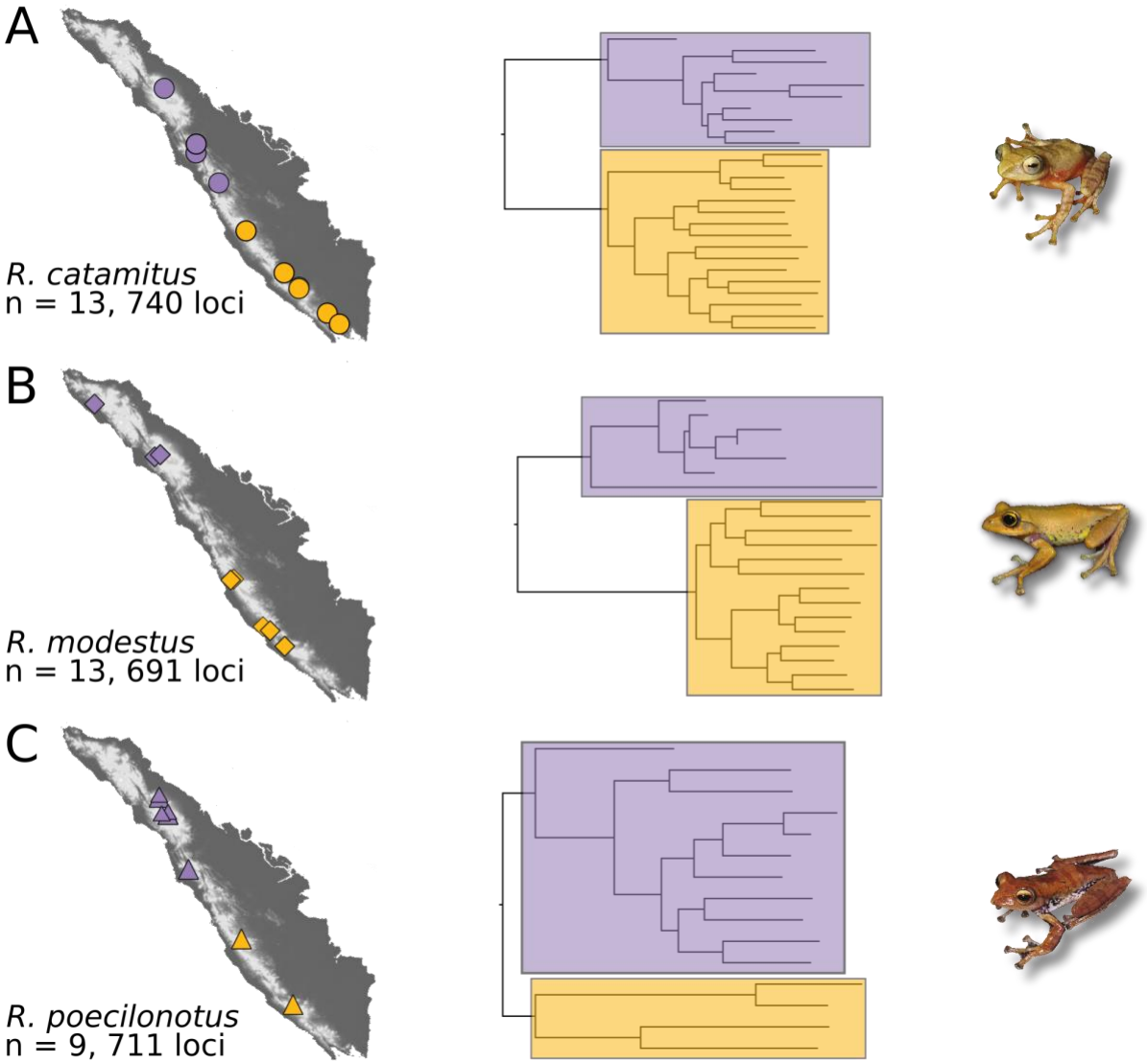

Figure 2: Sampling for the target capture data sets used in this study. The number of loci listed reflects the loci included in the full-locus data sets (see main text). Maps demonstrate the geographic location of each sample, and are accompanied by a phylogeny generated using RAxML v.8.2.11. Each element is colored to reflect northern and southern population assignments, with individuals pertaining to the northern population colored purple, and individuals pertaining to the southern population colored orange. Phylogenetic analyses were conducted on phased alleles, thus the number of tips in the phylogeny is twice the sample size listed under the maps. Maps and phylogenies correspond to A) *R. catamitus*, B) *R. modestus*, C) *R. poecilonotus*.

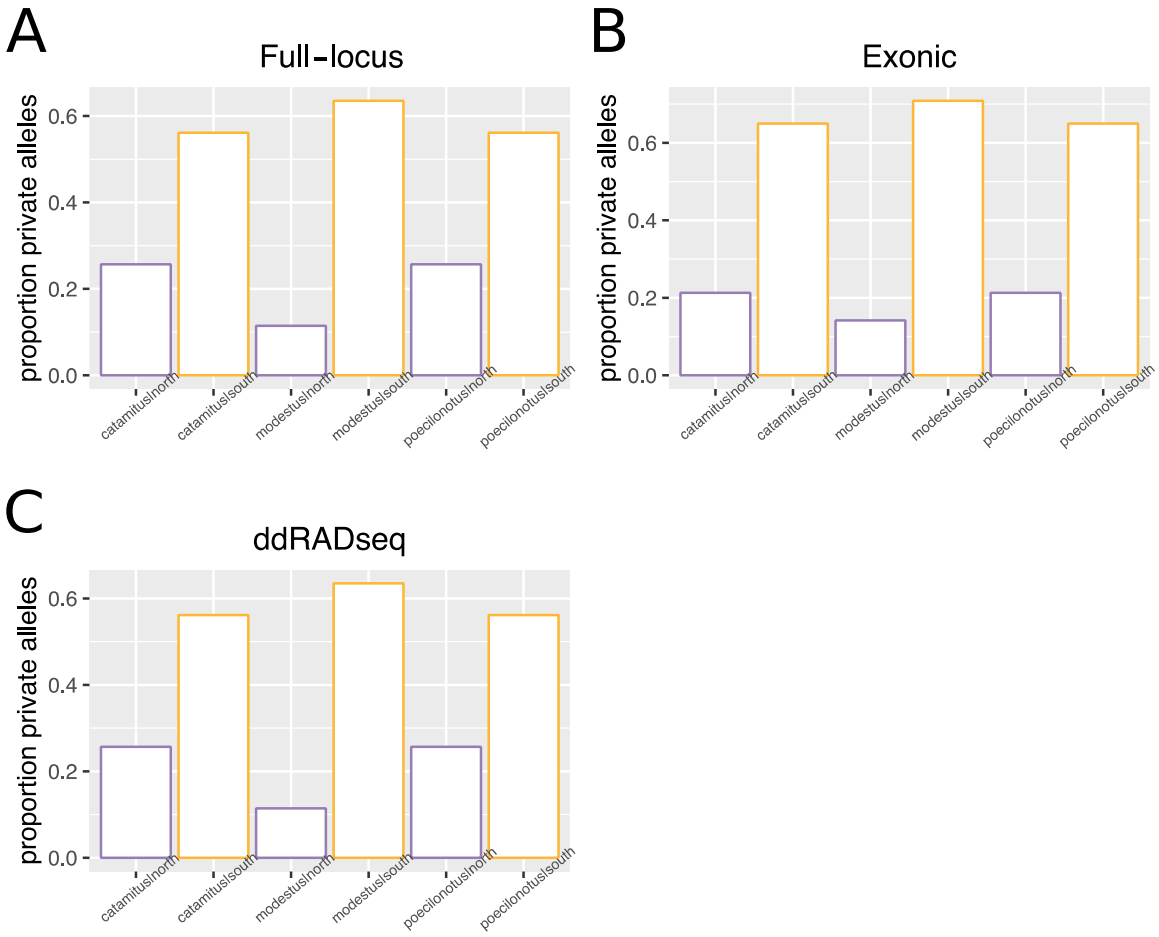

Figure 3: Proportion of private alleles for each datatype showing that southern populations exhibit higher levels of genetic diversity. Datatypes are as follows: A) full-locus, B) exonic, C) double-digest RADseq. Northern populations are colored purple, while southern populations are colored orange.

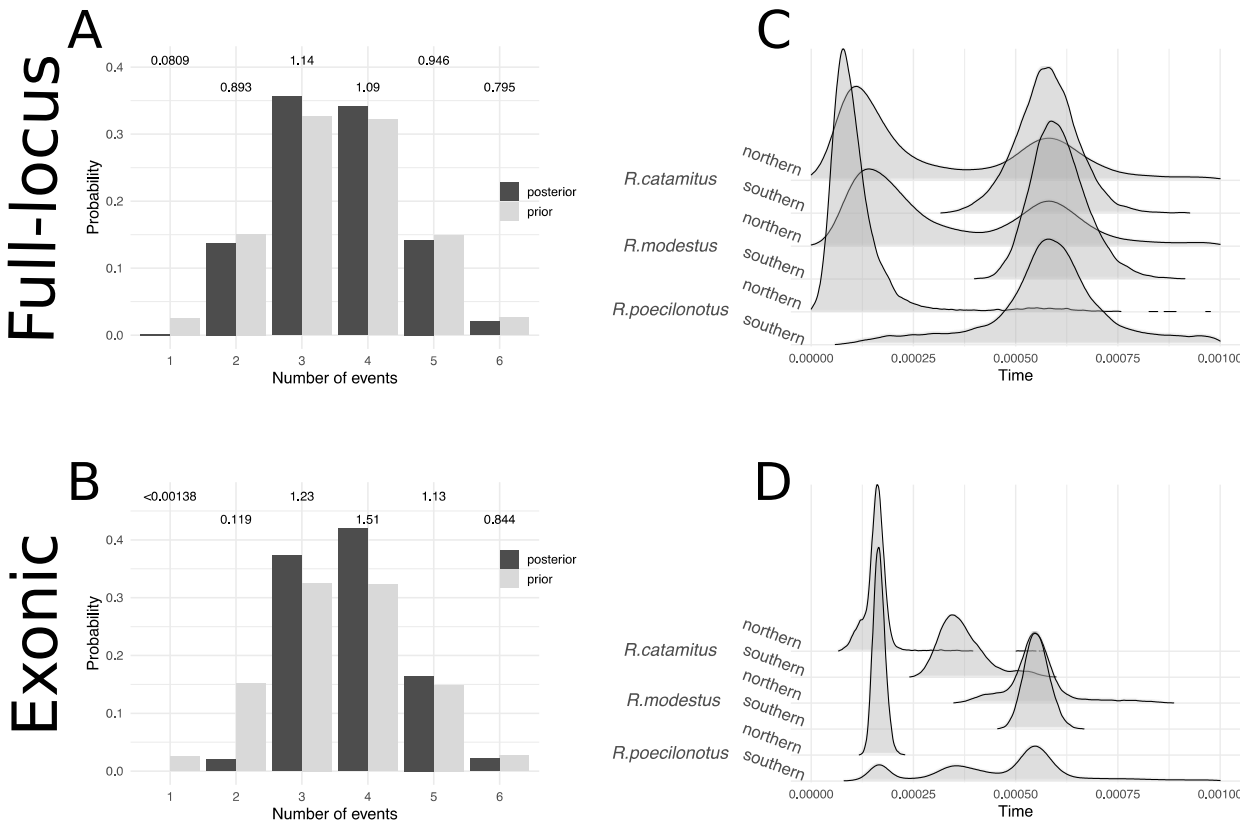

Figure 4: Temporal clustering of demographic events as inferred by ecoevolity v.0.3.2. A,B) Posterior (dark gray) and prior (light gray) probability for the number of demographic events, with the Bayes Factor above each set of bars, shown for the A) full-locus data set, B) exonic data set. C-D) Posterior distributions of estimated demographic event times for C) full-locus data set, D) exonic data set. Times are in units of expected substitutions per site, and were thus converted to years by dividing by the mutation rate of 1.42 x 10^{-9} substitutions per site per year.

Supporting Information

Table S1: Sample-level details on library preparation, hybridization reactions, raw reads, and final number of loci in alignments (available upon acceptance).

Table S2: Museum numbers and locality information for both target capture and ddRADseq samples included in this study (available upon acceptance).

Table S3: Population genetic parameter estimates for both the target-capture loci with all SNPs in a locus as well as only one SNP per locus (available upon acceptance).

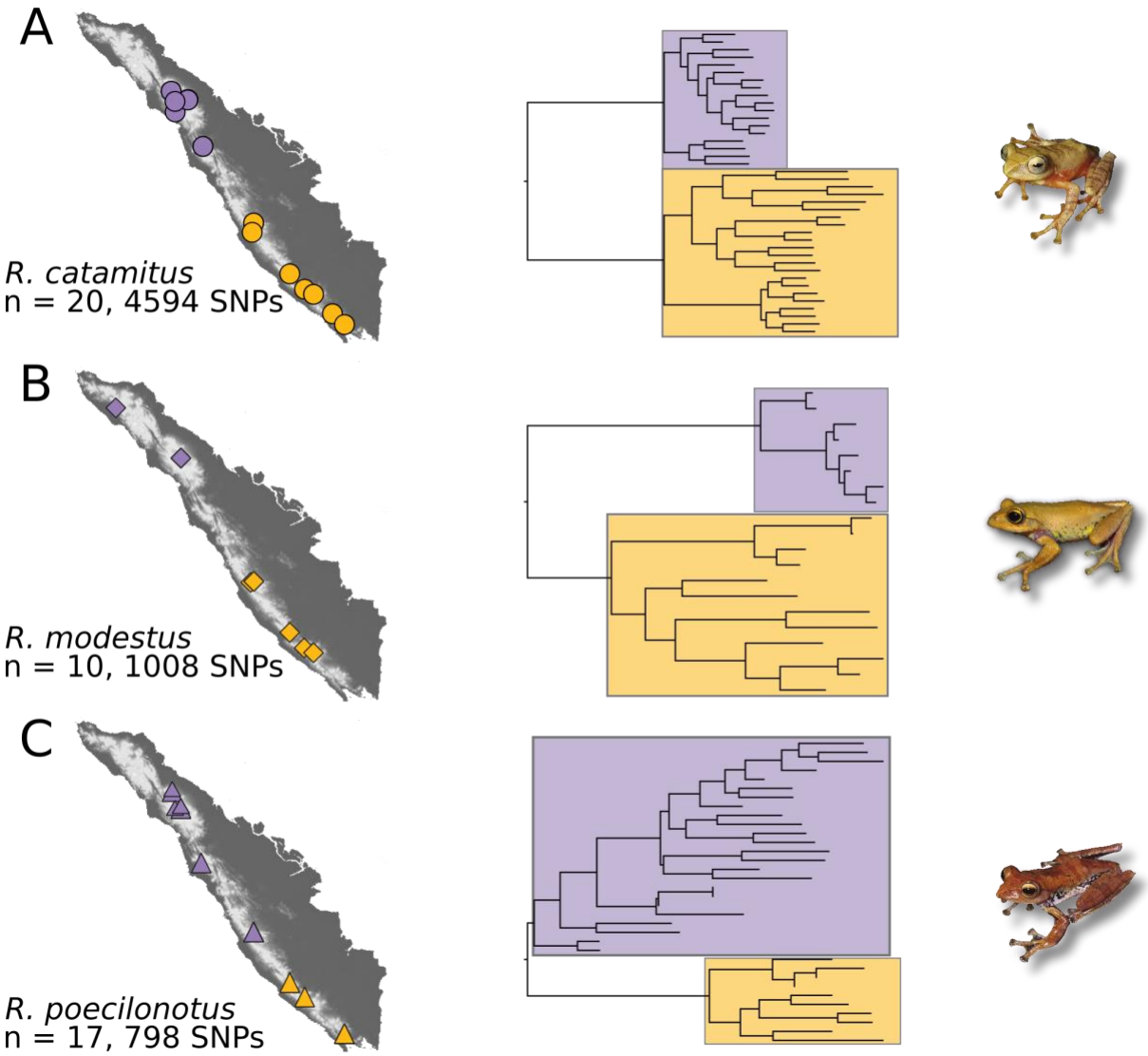

Figure S1: Sampling for ddRADseq data sets from O'Connell et al (2018a). Maps demonstrate the geographic location of each sample, and are accompanied by a phylogeny generated using RAxML v.8.2.11. Each element is colored to reflect northern and southern population assignments, with individuals pertaining to the northern population colored purple, and individuals pertaining to the southern population colored orange. Phylogenetic analyses were conducted on phased alleles, and thus the number of tips in the phylogeny is double the sample size listed under the maps. Maps and phylogenies correspond to A) *R. catamitus*, B) *R. modestus*, C) *R. poecilonotus*.

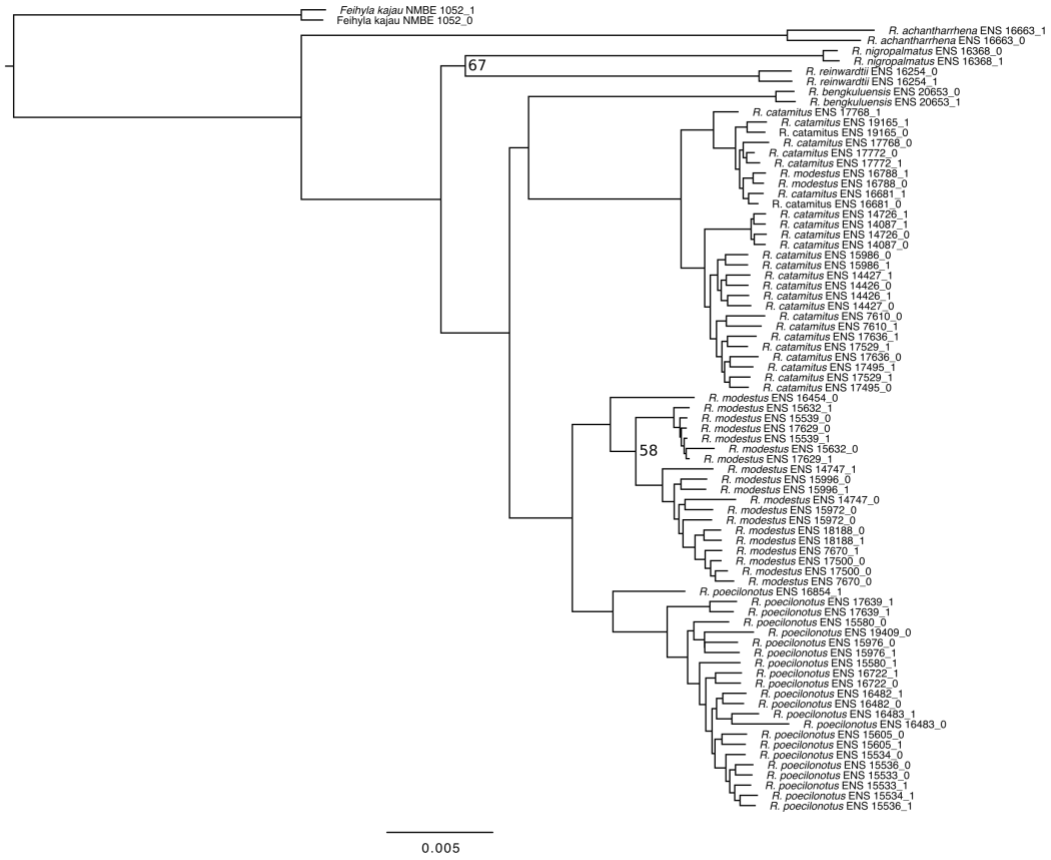

Fig. S2: Phylogeny of phased alleles for all samples included in the capture experiment (after removing failed individuals) generated using RAxML v.8.2.11 with 100 rapid bootstrap iterations. Nodal support below 100 is indicated. Analysis is based on 944 loci from the exonic data set, and recover phylogenetic relationships matching past studies (e.g. O'Connell et al., 2018a).

Exonic

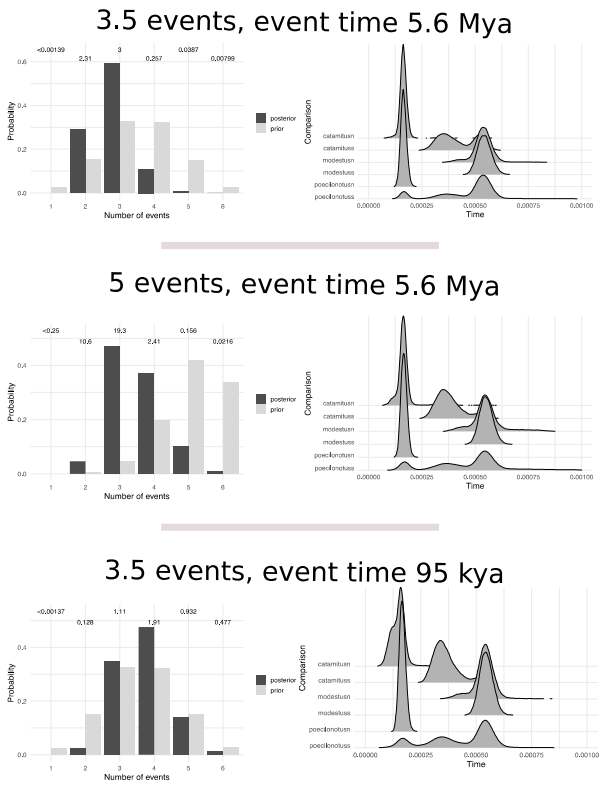

Figure S3: Examples of other ecoevolity outputs for the full-locus data set from some of our parameter optimization showing the effect of the prior on the concentration parameter on the prior and posterior support for the number of demographic events, but not the posterior distribution of event times. The number of events above each figure signifies the mean prior probability on that number of events, while the event time is the mutation-rate-converted rate of the exponential distribution on the event time prior.

Exonic

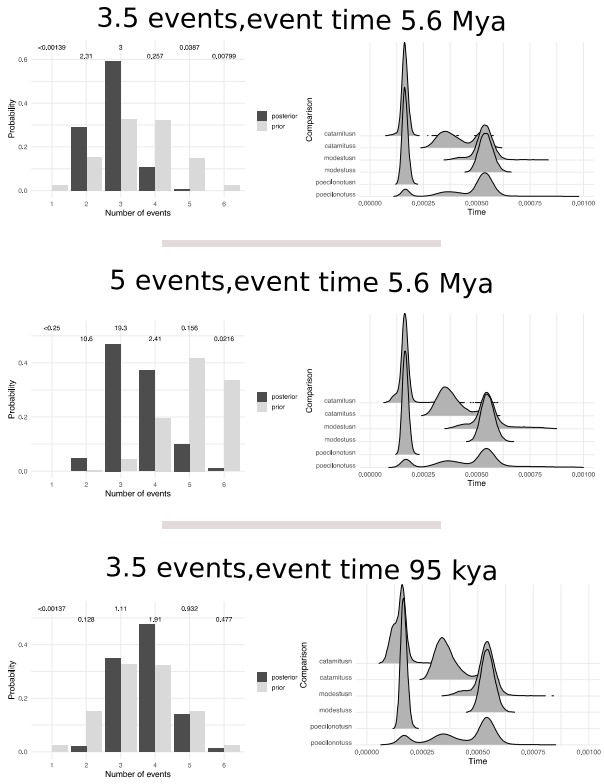

Figure S4: Examples of other ecoevolity outputs for the exonic data set from some of our parameter optimization showing the effect of the prior on the concentration parameter on the prior and posterior support for the number of demographic events, but not the posterior distribution of event times. The number of events above each figure signifies the mean prior probability on that number of events, while the event time is the mutation-rate-converted rate of the exponential distribution on the event time prior.

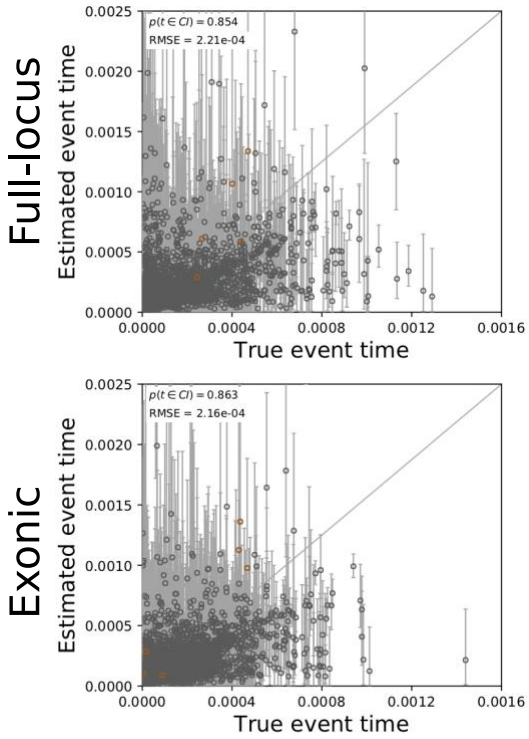

Figure S5: The accuracy and precision of estimates of demographic event times (in units of expected substitutions per site). Here we compare data simulated to match our empirical data for numbers of individuals, locus number, locus length, and levels of missing data. The full-locus data set is on the top row, while the exonic data set is on the bottom row. Each plotted circle and error bars represent the posterior mean and the 95% credible interval. Estimates for which the potential scale reduction factor was greater than 1.2 are highlighted in orange. Each plot contains 3,000 estimates (500 simulated data sets each with six time estimates). Each plot shows the root-mean-square error (RMSE) and the proportion of estimates for which the 95% credible interval contained the true value – ($p(t \in \mathrm{CI})$. Plots were generated using 'pycoevolity' v.0.2.4.

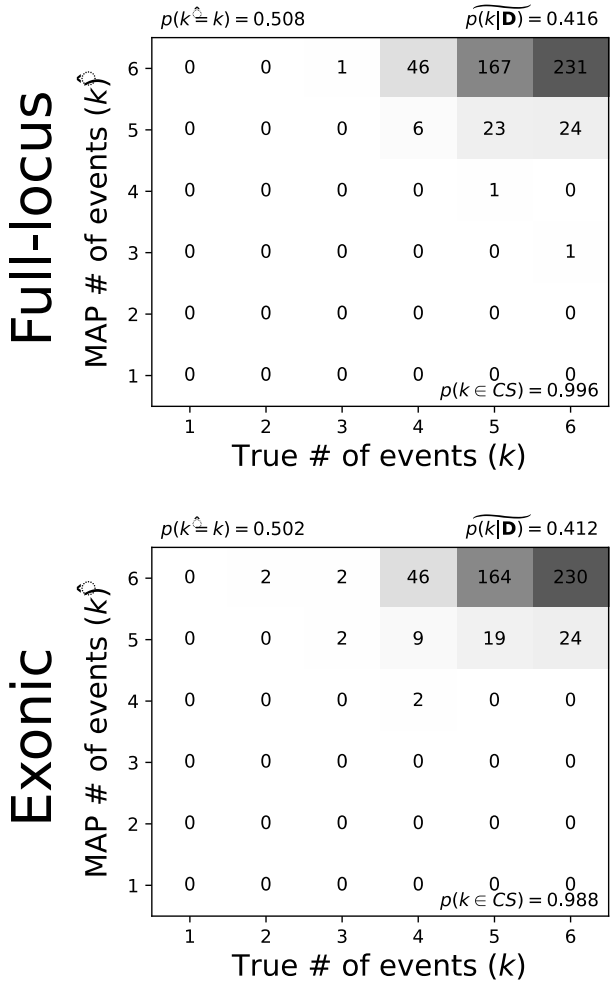

Figure S6: The performance of ecoevolity to estimate the true number of events using data simulated to match our empirical data. Each plot shows the results of the analyses of 500 simulated data sets, each with six demographic event estimates. The number of data sets that fall within the cells of the true verses estimated model is shown, and cells with more data have darker shading. The estimates are based on the model with the maximum *a posteriori* probability (MAP). For each plot, the proportion of data sets for which the MAP model match the true model is shown in the upper left hand corner, and the median posterior probability of the correct model across all data sets is shown in the upper right hand corner. The proportion of estimates for which the 95% credible interval contained the true value is shown in the bottom right corner. Plots were generated using 'pycoevolity' v.0.2.4.

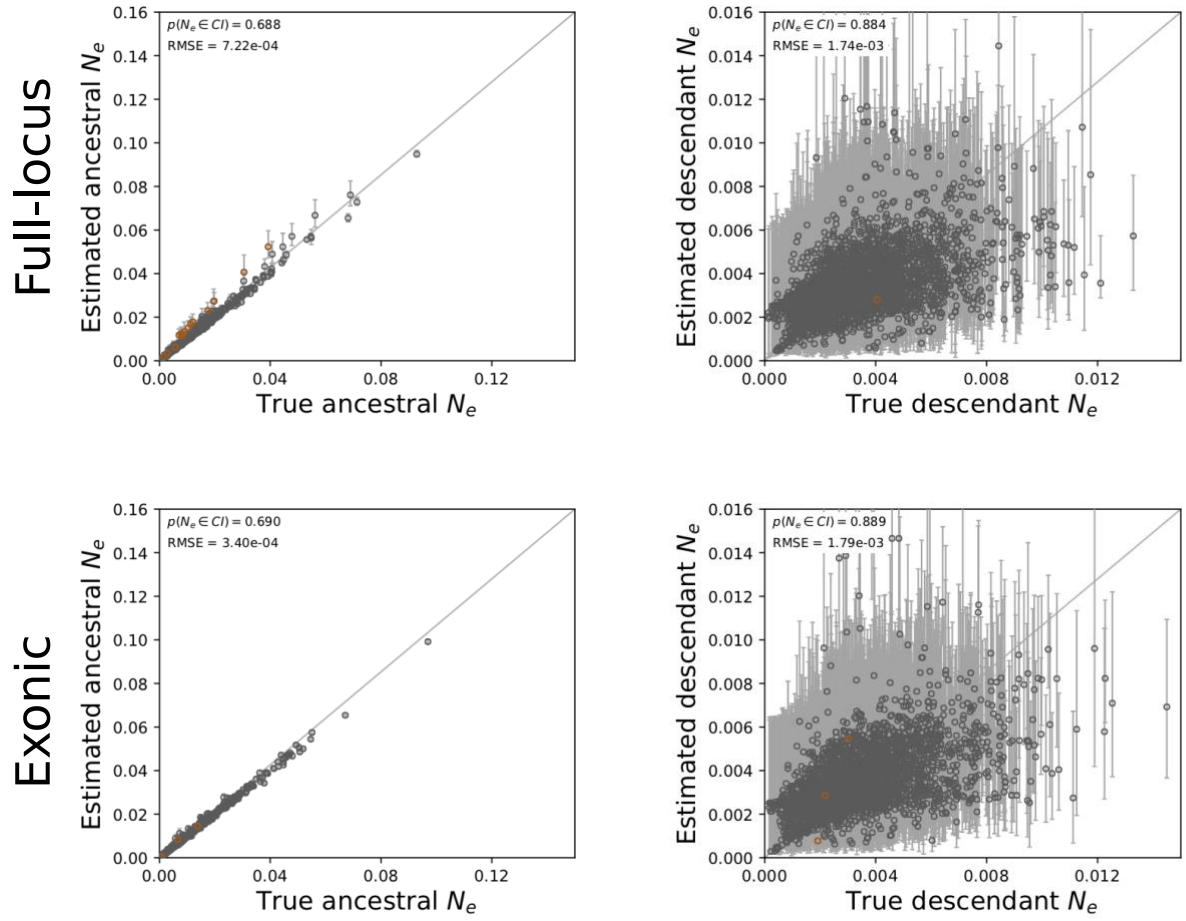

Figure S7 : The accuracy and precision of effective population size estimates for ancestral populations (left column) and descendent populations (right column). The full-locus data set is on the top row, while the exonic data set is on the bottom row. Each plotted circle and error bars represent the posterior mean and the 95% credible interval. Estimates for which the potential scale reduction factor was greater than 1.2 are highlighted in orange. Each plot contains 3,000 estimates (500 simulated data sets each with six time estimates). Each plot shows the root-mean-square error (RMSE) and the proportion of estimates for which the 95% credible interval contained the true value – ($p(t \in \mathrm{CI})$. Plots were generated using 'pycoevolity' v.0.2.4.

Additional supporting information

INTRODUCTION

A note on taxonomy of Rhacophoridae

Jiang et al. (2019) used 972 bp of mitochondrial sequence from 55 species and morphological data from the literature to revise the taxonomy of the genus *Rhacophorus*. In their paper they used phylogenetic analyses of the mitochondrial data to infer three well-supported clades within *Rhacophorus* which had been recovered in past studies (e.g. O'Connell et al. 2018a). They

divided *Rhacophorus* into three genera, applying the name *Rhacophorus s.s.* to the group of species encompassing most Sundaland taxa (including most of the Sumatran and Javan species). The clade that includes most of the taxa from Borneo (as well as *R. cyanopunctatus* from across Sundaland including on Sumatra), they assigned to the generic name *Leptomantis*. This genus was synonymized with *Rhacophorus s.l.* by Harvey et al. (2002) because it was non-monophyletic with respect to *Philautus* and the characters used to define it applied to members of *Rhacophorus s.s*. Finally, the clade including mostly East Asian taxa Jiang et al. (2019) assigned to the new genus *Zhangixalus*. Although several past studies have consistently recovered these three clades, the study by Jiang et al. (2019) contains a number of shortcomings that should be rectified before their new taxonomy is adopted.

First, they failed to sample all available sequences on Genbank (at least 68 at the time of O'Connell et al. 2018b), instead only including 55 of the 95 species described from the genus (amphibiaweb.org). Incomplete taxon sampling is known to influence phylogenetic estimation (Zwickl & Hillis, 2002), and this may have serious implications when revising whole genera based on very limited sampling. For example, the study failed to include any sequences of *R. cyanopunctatus*, although sequences from multiple landmasses are available on Genbank and were sampled by past studies (e.g. O'Connell et al. 2018a,b). In addition, with the availability of an abundance of nuclear data on Genbank (e.g. Chan et al. 2018; O'Connell et al. 2018a,b), it seems inappropriate at best to only sample mitochondrial data, particularly when assigning clades to genera. The primary issue for our study is that some taxa from Sumatra have been placed in the phylogeny in different locations in different studies. For example, Jiang et al. (2019) placed the *R. achantharrhena* clade as part of *Zhangixalus* with strong support, which was also recovered by Li et al. (2012) using only mitochondrial DNA. Chan et al. (2018) recovered a similar topology using nuclear and mitochondrial DNA, whereas O'Connell et al. (2018a,b) used nuclear and mitochondrial data to place the *R. achantharrhena* clade as sister to both the clade referred to as *Leptomantis* and that referred to *Zhangixalus*. Jiang et al. (2019) admit that the placement of the *R. achantharrhena* clade remains uncertain, but assign these species to their new genus, even though they do exhibit any of the characters used to define the new genus (see their Discussion). Due to the uncertainty of placing some of the Sumatran species in the revised taxonomic arrangement, we advocate for not adopting this new taxonomy until more comprehensive phylogenetic sampling is undertaken, specimens are examined to confirm the characters for each clade (they only used characters from the literature), and perhaps the phylogeny is better resolved using phylogenomic analyses rather than a few mitochondrial and nuclear genes.

MATERIALS AND METHODS

Details on ecoevolity parameter variations

We applied a Dirichlet process with a concentration parameter values fixed at 2.62 on the event model prior (estimate = false), which corresponds to at least half the prior probability being placed on 3.5 demographic events, although we also tested prior values of 12 (5 events) and 20 (5.3 events). We applied an exponential distribution to the event time prior with a rate of 1000 (corresponding to a mutation-rate converted value in years of ~500 Kya), but also tested values of 6000 (~95 Kya), 800 (800 kya), 500 (~1.4 Ma), and 100 (~5.6 Ma). Under global comparison

settings, we set genotypes = haploid, and set constant sites removed = false, and equal population sizes = false. For the prior on the current population size, we used a theta = 0.004 (calculated from the full-locus data set from each species) to place a prior value of 0.001 with a gamma distribution (shape = 3.5, scale = 0.001). We visualized our prior distributions using (https://github.com/ivanprates/2018_Anolis_EcolEvol/tree/master/scripts), ensuring that the gamma distribution encompassed our starting value. For the root relative population size, we used our δaδi results to apply population-specific exponential distributions. On the northern populations of *R. catamitus* and *R. modestus* we applied an exponential distribution with a mean = 2, suggesting that the ancestral population was twice as large as the current population (contraction scenario), and on the southern populations applied an exponential distribution with a mean = 0.5, such that the current population is twice the size of the ancestral population (expansion). In *R. poecilonotus* we applied the inverse parameters. In all cases we allowed the parameter to be estimated. We also tested the inverse of these size priors to test their sensitivity on analyses but found no difference in the posterior estimates.

RESULTS

Target capture efficiency at the generic level

We filtered out samples that captured fewer than 20% of loci (<190 loci), leaving 45 samples for downstream analyses (Table S1). Our filtered sampling included seven nonimal species from across the *Rhacophorus* phylogeny including *R. achantharrhena* (n = 3; mean loci captured in exonic data set = 592), *R. bengkuluensis* (n = 1; 917 loci), *R. nigropalmatus* (n = 1; 898 loci), *R. reinwardtii* (n = 1; 877 loci), *R. catamitus* (n = 13; 878 loci), *R. modestus* (n = 15; 887 loci), *R. poecilonotus* (n = 10; 819 loci), and one species from a closely related genus, *Feihyla kajau* (n = 1; 699 loci). Generally, our probe set worked well across the genus and with the outgroup sample, recovering 950/951 target loci across a minimum of three samples. To illustrate, we recovered an average of 887 loci (765–950) for *R. modestus* the species from which transcriptome-based probes were designed, while the outgroup *F. kajau* retained 699 loci across ~36 Ma divergence (O'Connell et al. 2018b).

Population structure at the generic level

Our ML phylogeny of all species matched closely with that of O'Connell et al. (2018b) based on multi-locus Sanger sequence data (Fig. S2). We inferred *R. achantharrhena* as sister to all other Sumatran and Javan *Rhacophorus*. We recovered *R. nigropalmatus* as sister to *R. reinwardtii*, and these two species were sister to the clade that included the focal Sumatran species. Within the focal Sumatran clade, we inferred *R. bengkuluensis* from Java as sister to *R. catamitus*, and these species were sister to *R. modestus* and *R. poecilonotus*. Only two nodes had less than 100% bootstrap support: the relationship between *R. nigropalmatus* and *R. reinwardtii*, and the north/south split in *R. modestus*.

REFERENCES

Chan, K. O., Grismer, L. L., & Brown, R. M. (2018). Comprehensive multi-locus phylogeny of Old World tree frogs (Anura: Rhacophoridae) reveals taxonomic uncertainties and potential cases of over-and underestimation of species diversity. *Molecular Phylogenetics and Evolution*, *127*, 1010-1019.

Jiang, D., Jiang, K., Ren, J., Wu, J., & Li, J. (2019). Resurrection of the Genus *Leptomantis*, with Description of a New Genus to the Family Rhacophoridae (Amphibia: Anura). *Asian Herpetological Research, 10*, 1–12.

Li, J. T., Li, Y., Klaus, S., Rao, D. Q., Hillis, D. M., & Zhang, Y. P. (2013). Diversification of rhacophorid frogs provides evidence for accelerated faunal exchange between India and Eurasia during the Oligocene. *Proceedings of the National Academy of Sciences*, *110*, 3441-3446.

O'Connell, K. A., Hamidy, A., Kurniawan, N., Smith, E. N., & Fujita, M. K. (2018a). Synchronous diversification of parachuting frogs (Genus *Rhacophorus*) on Sumatra and Java. *Molecular Phylogenetics and Evolution*, *123*, 101–112.

O'Connell, K. A., Smart, U., Smith, E. N., Hamidy, A., Kurniawan, N., & Fujita, M. K. (2018b). Within-island diversification underlies parachuting frog (Rhacophorus) species accumulation on the Sunda Shelf. *Journal of Biogeography*, *45*, 929–940.

Zwickl, D. J., & Hillis, D. M. (2002). Increased taxon sampling greatly reduces phylogenetic error. *Systematic Biology*, *51*, 588–59.